Emerging Trends in Scientific Research

Volume – 2

Chief Editor

Dr. Dhondiram Tukaram Sakhare
Assistant Professor, UG, PG & Research Centre, Department of Chemistry, Shivaji Arts, Comm. & Science College, Kannad, Aurangabad, Maharashtra, India

Integrated Publications
New Delhi

Published By: Integrated Publications

Integrated Publications
H. No. - 3 Pocket - H34, Sector - 3,
Rohini, Delhi-110085, India
Phone No. – 9911215212
Email – printintegrated@gmail.com

Chief Editor: Dr. Dhondiram Tukaram Sakhare

Publication Year: 2022

Pages: 107

ISBN:

Book DOI: https://doi.org/

Price: ₹ 613/-

Contents

Chapter - 1
Drug Repurposing: A New Paradigm in Pharmaceutical Drug Discovery

Authors

MV Kumudhavalli
Department of Pharmaceutical Chemistry (Including Pharmaceutical Analysis) Vinayaka Mission's College of Pharmacy, VMRF (DU) Yercaud main Road, Kondappanaickenpatty, Salem. Tamil Nadu, India

M Sivaramakrishnan
Department of Pharmaceutical Chemistry (Including Pharmaceutical Analysis) Vinayaka Mission's College of Pharmacy, VMRF (DU) Yercaud main Road, Kondappanaickenpatty, Salem. Tamil Nadu, India

S Rajakumaran
Department of Pharmaceutical Chemistry (Including Pharmaceutical Analysis) Vinayaka Mission's College of Pharmacy, VMRF (DU) Yercaud main Road, Kondappanaickenpatty, Salem. Tamil Nadu, India

G Sundar
Department of Pharmaceutical Chemistry (Including Pharmaceutical Analysis) Vinayaka Mission's College of Pharmacy, VMRF (DU) Yercaud main Road, Kondappanaickenpatty, Salem. Tamil Nadu, India

M Kumar
Department of Pharmaceutical Chemistry (Including Pharmaceutical Analysis) Vinayaka Mission's College of Pharmacy, VMRF (DU) Yercaud main Road, Kondappanaickenpatty, Salem. Tamil Nadu, India

Chapter - 1

Drug Repurposing: A New Paradigm in Pharmaceutical Drug Discovery

MV Kumudhavalli, M Sivaramakrishnan, S Rajakumaran, G Sundar, and M Kumar

Abstract

The practise of identifying new therapeutic applications for old/existing/available medications is known as drug repurposing (DR). It's an excellent method for discovering and developing novel pharmaceutical compounds with a wide range of pharmacological and therapeutic uses. Several pharmaceutical firms have used the medication repositioning technique to produce new pharmaceuticals based on the discovery of novel biological targets in their drug development programmes in recent years. This strategy is highly effective, saves time, money, and has a low failure rate. It increases the therapeutic value of a medicine, increasing its chances of success. As a result, drug repositioning has grown in popularity as a viable alternative to conventional drug development. Using standard or de novo drug development procedures, identifying new molecular entities (NME) involves time and money. To develop/identify innovative applications for medicinal substances, drug repositioning combines the efforts of activity-based or experimental and in silico-based or computational methods.

Keywords: Drug repurposing, Drug discovery, Clinical trials.

Introduction

Everything about science is changing in the Information Age. This data deluge is affecting experimental, theoretical, and computational sciences, and a fourth, "Data-intensive" science paradigm is emerging, New paradigm of research, the process of recovering "Source Data" from main scientific literature.

We are drowning in Data, but starving for Knowledge" – Unknown

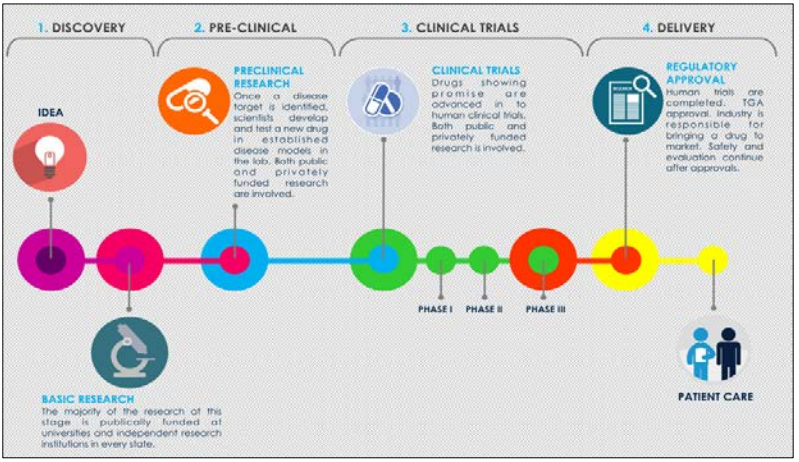

Despite increased research and development spending, the number of new authorised pharmaceuticals has dropped dramatically in recent years. According to data from a survey of nine multinational pharmaceutical companies, the FDA authorised only two novel molecular entities from all of these businesses in 2010, a very dismal return on their $60 billion investment [1]. It's no secret that the pharmaceutical R&D industry requires more tools to minimise discovery and development expenses. According to one study, the cost of bringing a medicine to market can range from $1 billion to $2.6 billion [2]. In comparison, the typical cost of bringing a mobile app to market in the software business is less than one million dollars [3].

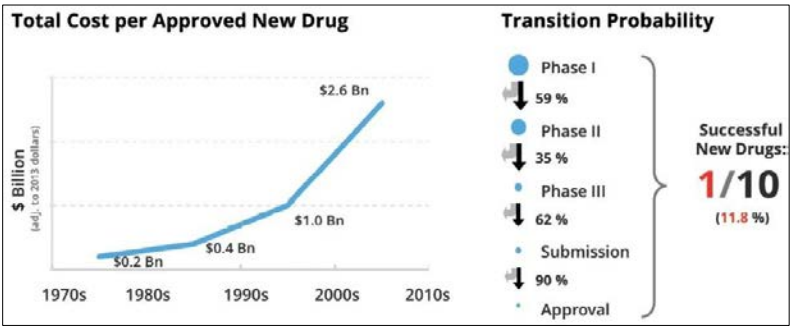

The Tufts Center for the Study of Drug Development (CSDD) undertakes regular cost evaluations of drug development, with the most current estimate of the average cost of attaining marketing clearance coming in at little under $2.6 billion. There are a number of reasons that contribute to the astronomical pricing. Over $1.4 billion in out-of-pocket expenditures and

over $1.1 billion in 'Time costs,' or investment returns missed while a treatment is being developed, were estimated by Tufts throughout the industry.

By merging distinct and heterogeneous data sources from the genomes and biological domains, in-silico technologies such as data mining, machine learning, and network-based approaches present a once-in-a-lifetime chance to foresee all possible drug repositioning candidates [14]. These techniques have been used to develop prediction models based on existing data such as protein targets, chemical structure, or phenotypic data such as side-effect profiles, gene expression, and so on.

While improvements in computational sciences have allowed new tools and methodologies to be applied to systems biology data, these datasets have also sparked fundamental study on more challenging challenges [10]. Many modalities of Drug Repurposing or Repositioning strategies have evolved as a result of this hybrid way of using computational tools and experimental screens.

Depending on the type of drug discovery (drug-based or disease-based), target-based, expression-based, knowledge-based, chemical structure-based, pathway-based, and mechanism-of-action-based computational drug repositioning methods can be classified as target-based, expression-based, knowledge-based, chemical structure-based, pathway-based, and mechanism-of-action-based methods [11].

In this review paper, we briefly discuss recent improvements in computational approaches and tactics that we studied, appraised, and used to drug-disease data for drug repositioning research. Medication repurposing, also known as drug repositioning, is a drug development process that involves repurposing previously authorised pharmaceuticals for new medicinal purposes. It occurs when a drug is repurposed to treat a different condition. The knowledge that shared biological pathways contribute to a variety of illnesses underpins drug repositioning.

Drug repositioning provides several benefits over typical de novo drug discovery strategies, including the ability to dramatically cut development costs and time, as well as the removal of Phase I clinical trials in many cases.

Advantages and Disadvantages of Drug Repositioning

1. Safety Advantage

Existing medications that have been authorised or demonstrated to be safe in late-stage studies but have failed to fulfil the end points of their

original planned applications can take advantage of the lower development risk by expanding into new indications. They can do so if they can show that they are efficacious in new indications and that they are sufficiently distinct from standard of treatment.

When these medications enter clinical trials, they compete with non-repositioned treatments on effectiveness rather than safety. Because safety accounts for around 30% of therapeutic failures in clinical trials, repositioned pharmaceuticals have a considerable development advantage.

2. Money Savings Advantage

According to a recent analysis based on a survey of 30 pharmaceutical and biotechnology companies, the average cost of relaunching a repositioned medicine is $8.4 million, whereas the average cost of relaunching a new formulation of an existing drug in its original indication is $41.3 million. The medicine has now reached the market in both circumstances. The expense of market entry for a repositioned medicine vs a new drug, on the other hand, is just astonishing.

Given that the latter costs an average of more than $1.3 billion, bringing a repositioned medicine to market appears to cost around 160 million times less than the current NCE/NME development standard. Even if the difference is a hundred million dollars or more, from a purely financial standpoint, repositioning is in a different league from the expenditure required to launch a new medicinal product on the market.

3. Market Potential Advantage

Not all medications are blockbusters, but several have been repositioned to attain this status. Celgene's Thalomid®, a repositioned thalidomide, and its derivative Revlimid® are two outstanding examples (lenalidomide). Celgene's aggregate worldwide revenue stream from these two repositioned medications is more than $2.8 billion. Although one should not assume that the financial success of one repositioned medicine would instantly translate to the financial success of all repositioned pharmaceuticals, it is difficult to dismiss the commercial potential of repositioning as a strategy.

Many elements influence market success, including market demand, competition, difference, a great product, IP obstacles, payer acceptance, compliance, and a successful market strategy. These variables apply to repositioned pharmaceuticals in the same manner that they do to NCE/NME drugs, thus it's vital to remember that repositioned drugs have no intrinsic properties that restrict their market potential.

Existing medications can be repurposed to treat a variety of conditions for which there is presently no effective treatment. Repurposing current medications, according to Carlos Telleria, an ovarian cancer researcher at McGill University in Canada, has the potential to "transform cancer into a curable chronic condition." Patients with the approximately 8,000 uncommon disorders may also find relief, as experts estimate that virtually all of these ailments might be treated with currently available medications. Drug repurposing also has tremendous promise for Alzheimer's disease and many other central nervous system illnesses for which no viable therapies exist.

New technologies are becoming more widely available, potentially revolutionising how scientists select current medications for repurposing. New applications for existing medications have traditionally been discovered by physician inquiry, selective testing of particular pharmaceuticals in cell-based or animal disease models, or simply by chance. However, new advancements in chemo informatics, genetic screening, and data mining are transforming this approach into one that is more focused, methodical, and cost-effective.

Benefits for Patients

For patients, repurposing existing medications makes a lot of sense. The safety profile of a repurposed medication is far more understood than that of a fully new therapy. Patients are therefore safer when a known medicine is repurposed rather than a novel treatment with little or no track record.

In repurposed medications, side effects and drug interactions have previously been recognised, allowing clinicians to identify individuals who are more likely to have adverse effects and make a better educated cost-benefit judgement about whether a prescription is appropriate for a certain patient. It will also assist doctors in determining which medication interactions should be avoided.

Painstaking R&D required Repurposing a Drug

It's not just a matter of altering the packaging and transporting it to pharmacies when it comes to repurposing. It nearly usually comes after a lot of research and clinical trials. As a result, it is a costly and dangerous process that needs suitable incentives, such as intellectual rights.

The FDA, for example, restricts pharmaceutical corporations from promoting medications for 'off-label' applications in the United States. While medical physicians are not prohibited from prescribing medications for

unapproved reasons, regulatory clearance encourages prescriptions for secondary medical purposes.

"Without clinical evidence confirming that drug's therapeutic benefit for the new indication, physicians are far less inclined to prescribe it for that new usage," says Benjamin Roin, assistant professor of technology innovation, entrepreneurship, and strategic management at MIT Sloan. Obtaining regulatory approval for a new use also increases access by allowing third-party payers to add it on their reimbursement lists.

It's a frequent misconception that creating a recognised medicine for a new application will be far cheaper than inventing a single new chemical entity." Of course, setting up and executing clinical trials is an expensive procedure that may cost tens or even hundreds of millions of dollars. At the very least, they usually take many years to finish.

Although most medication repurposing R&D projects have already completed pre-clinical and Phase 1 clinical trials, it is still a significant expenditure to complete the remaining clinical studies required for marketing authorisation. As a result, patent protection is critical.

"A common expectation is that repurposing an existing drug will be less expensive than developing a single new chemical entity," says Hermann Mucke, a pharmaceutical industry specialist. "The most expensive components of a drug development programme, late-stage studies, apply to repurposed development to the same extent as unsuccessful drugs."

In academics, there is a common belief that pharmacological repurposing is just about finding new targets for existing therapies. When evaluating medication repurposing potential, several factors should be examined, including illness relevance, side effect tolerability for the new use, and intellectual property position. All of these points are covered in the medication repurposing flowchart shown below, which is contextualised in the sections that follow.

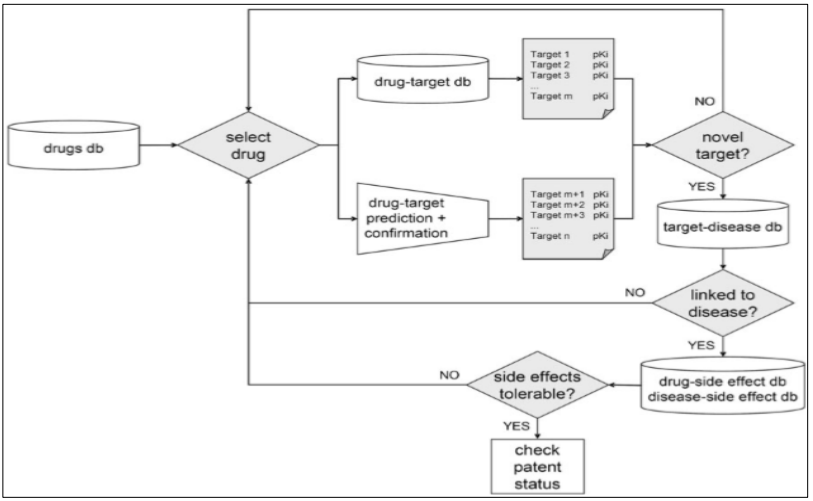

This viewpoint is not shared by all countries. With its explicit ban in section 3(d) of the Indian Patents Act, India does not provide patent protection for innovative applications of recognised pharmaceuticals. This exclusion is based on the belief that new uses do not meet important patentability requirements such as innovation and non-obviousness. However, patent protection has been critical in the development of successful repurposed pharmaceuticals that provide significant advantages to patients.

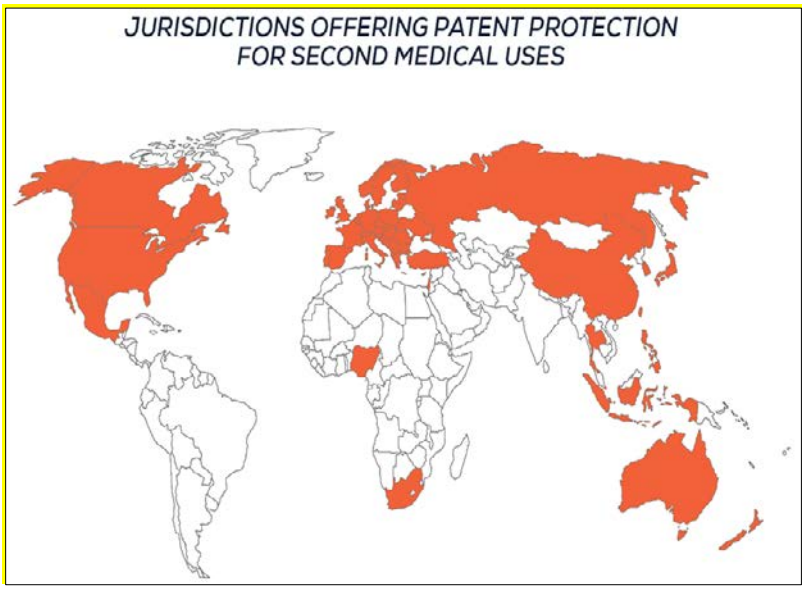

Need of Drug Repurposing

The drug repurposing strategy is supported by a number of experimental and clinical criteria [13]. One of the most prevalent target-directed preclinical drug development scenarios [14] is to optimise main target binding affinity while lowering affinity for "secondary targets" (i.e., selectivity). Drug pharmacokinetics and safety profiling, as well as target profiling of stated drug candidates for other, unrelated target classes, are routinely missed in such endeavours. COX-2 selective medicines [16], which were less active on the related enzyme cyclooxygenase 1, were found after the relevance of cyclooxygenase 2 (COX-2) in inflammation and pain was recognised [15]. (COX-1). On this basis, celecoxib (Celebrex®) was created.

When compared to COX-1, this compound is an order of magnitude more powerful [17]. According to the pharmaceutical label [18], it can be used to treat osteoarthritis, rheumatoid arthritis, juvenile rheumatoid arthritis, pain, ankylosing spondylitis, and dysmenorrhea and it appears to have less side effects than valdecoxib (Vioxx®), another COX-2 selective chemical. Vioxx was withdrawn from all markets by Merck & Co. [19] in 2004. Celebrex is still advertised by Pfizer and other pharmaceutical corporations. However, the lack of complete knowledge of drug–target interaction profiles [20], especially for older drugs, allows for the repurposing of already-approved drugs for new therapeutic indications by identifying biologically and clinically relevant affinities for new targets that play a key role in those indications.

Novel computational algorithms that can predict the target profile of small compounds with increasing recall and precision have greatly expanded the target space that can be examined, making it easier to find new targets for existing medications [21–23]. Another benefit is that the NME under consideration for repositioning is already authorised, eliminating the requirement for phase I and phase II clinical studies.

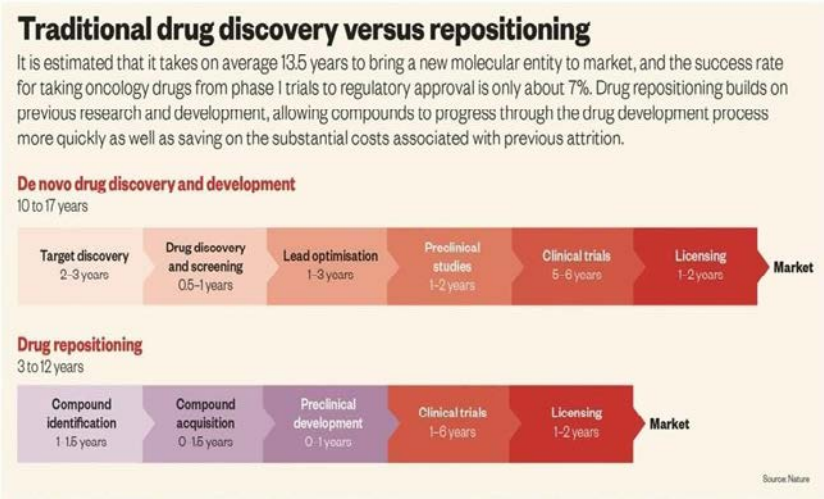

This is more likely to be the case when medications are repurposed at a dose that is similar to or lower than the maximum dose previously permitted by regulatory regulators [24]. Due to a substantial body of clinical data and experience obtained in phase III (efficacy) and phase IV (post-marketing) studies, the drug's profile in terms of adverse events, long-term and chronic toxicity, and on- and off-label effects is well characterised.

A large literature corpus for a specific treatment is frequently considered as favourable because, despite shortcomings, the clinical observation and monitoring required (especially in high-risk circumstances) is feasible. When an older drug is repurposed, it's thought that all of the costs involved with its production (including any possible hazardous waste) have been covered, making the therapeutic treatment of new indications economically viable. Last but not least, numerous large pharmaceutical companies have looked into repurposing as a way to extend the patent life (i.e., market exclusivity) for profitable medicine franchises.

Overall, the lack of data completeness during the preclinical phases, along with the collection of safety and efficacy data over the different clinical phases, creates a plethora of medication repurposing prospects. As a result, gathering and releasing as much data on the target profile of medications as feasible public would restrict the possibilities of repurposing from rivals.

What can be Repurposed?

The intellectual property landscape is a fascinating aspect of the de-risking strategy for pharmaceuticals that have already been licensed.

Medications whose patent rights on the topic and/or indication have expired are typically the target of drug repurposing. The availability of commercial chemical libraries made up of off-patent drugs has tremendously aided this method [25]. Completely innovative therapeutic uses are researched for those medications that are still covered by patents. Some may claim that market exclusivity requires patents on substance formulations.

Unless selectivity is not a problem, it is impossible to expect effective repositioning for a restricted therapeutic domain for more recent drugs that have been tuned for a long time for a specific target (or indication). More complicated therapeutic areas, such as the central nervous system, which is mostly tied to aminergic GPCRs, and oncology, which is primarily linked to kinases, are simpler to find for authorised medications since there is a larger number of targets and pathways that may be perturbed by NME.

Furthermore, because various target families have been proven to have varied amounts of cross-pharmacology, the chance of extremely similar ligands binding two unique targets, also known as cross-pharmacology, must be examined for the principal target(s) of a marketed medicine. In comparison to enzymes, ligand-gated ion channels, and nuclear receptors, GPCRs exhibit a higher degree of cross-pharmacology among their members. Furthermore, cross-pharmacology has been discovered between several GPCRs and non-GPCR proteins [27]. Given that several GPCRs are connected to many therapeutic areas (see above), medicines targeting aminergic GPCRs might be a good place to start when it comes to medication repurposing. Indeed, at least ten of the 26 newly evaluated repurposed medicines (38 percent) have known interactions with aminergic GPCRs.

Tools used for Drug Repurposing

Name	Class	Input	Output	Description	Weblink
Biovista	Static	Biological Knowledge	Gene-protein relation ships	A mining framework to extract gene-Protein relationships	http://www.biovista.com/
Biowisdom	Static	Ontology	Drug-disease , drug-target relationships	A platform to discover novel biological entity relationships.	http://www.biowisdom.com
Facta+	Static	Tekst	Abstracts and linked concepts	A system to find associated concepts based	http://www.nactem.ac.uk/facta /ceptsbased on a

				on a user query	user query
Edgar	Static	UMLS Terms	Drug-Gene relationships	A system to Extract relationships between drugs and genes involved in cancer using syntactic analysis	https://www.sec.gov/
Poly Search	Dynamic	Bio-Entities	Drug disease, Drug-gene relationships	A web service to extract links Between biological terms	http://wishart.biology.ualberta. ca

Conclusions

While the National Institutes of Health [28] is paying more attention to drug rescue and repurposing, this policy is not without hazards, particularly for the industrial sector. Indeed, when all relevant aspects are taken into account, drug repurposing may end up being quite expensive, further depleting the pharmaceutical industry's already limited resources.

On the one hand, the majority of drugs are the result of a protracted optimization process aimed at enhancing affinity and selectivity (among other things) for a single key target. As a result, the efficacy of novel targets uncovered for existing drugs is likely to be lower than the potency of the initial target. As a result, repurposing efforts should be directed towards a target/indication that was not intentionally counter-selected during the first project. It may be hard to show superiority in terms of effectiveness and safety (phases III and IV) if alternative medicines for that indication have already been licenced [29].

Target–disease relationships are not always totally trustworthy, according to a recent reproducibility study of 67 target validation studies [30]. As a result, the hazards of having a second-in-class medicine with lesser potency that isn't clearly related to a specific use should be carefully weighed. On the other hand, one should keep in mind that existing methodologies of suggesting medications for repurposing have a low specificity (in a statistical sense).

Recent academic interest in this topic has resulted in the publishing of a large list of drugs that might be repurposed for a variety of conditions, including TB [31], breast and prostate cancer, and myelogenous leukaemia [32]. This academic tendency has two (negative) consequences. This

knowledge is still regarded "prior art" since it is presently in the public domain, even if it has been empirically proven. This basically nullifies intellectual property protection and future investment in that particular combination of drugs, targets, or therapeutic indications.

It also tarnishes the credibility of computational methods to drug repurposing, as many of these suggestions are unlikely to gain regulatory clearance, which is still the most important requirement for drug repurposing success. Following up on all of the repurpose candidates who have been claimed looks to be impracticable. Rather, demonstrating the use of all potential repurposing drugs for a single application will very probably be a time-consuming and expensive process.

Taking all of the above into account, an ideal candidate for a repurposing initiative would be an off-patent safe drug with a novel target identified, affinity within the maximum recommended therapeutic dose for an already-approved indication, and strong evidence linking it to a therapeutically unmet need or rare disease.

References

1. Innovation in the pharmaceutical industry: New estimates of R&D costs, Joseph A. DiMasi, Henry G. Grabowski, Ronald W. Hansen, Journal of Health Economics, 2016.
2. A guide to drug discovery: Trends in development and approval times for new therapeutics in the United States, Janice M. Reichert, Nature Reviews Drug Discovery, 2003.
3. Clinical development success rates for investigational drugs, Michael Hay, David W Thomas, John L Craighead, Celia Economides, Jesse Rosenthal, Nature Biotechnology, 2014.
4. Kola I, Landis J. Can the pharmaceutical industry reduce attrition rates? Nature Reviews Drug Discovery. 2004;3:711-715.
5. Pammolli F *et al*. The productivity crisis in pharmaceutical R&D. Nature Reviews Drug Discovery. 2011;10:428-438.
6. Paul SM *et al*. How to improve R&D productivity: the pharmaceutical industry's grand challenge. Nature Reviews Drug Discovery. 2010;9:203-214.
7. Herper M. The Truly Staggering Cost of Inventing New Drugs. Forbes, 2012.
8. Linder M. Clinical attrition due to biased preclinical assessments of potential efficacy. Pharmacology and Therapeutics. 2007;115:148-175.

9. Munos B. Lessons from 60 years of pharmaceutical innovation. Nature Reviews Drug Discovery. 2009;8:959-968.

10. Prathipati P, Mizuguchi K. Systems Biology Approaches to a Rational Drug Discovery Paradigm. Curr.Top. Med. Chem. 2015;16:1009-1025.

11. Li YY, Jones SJM. Drug repositioning for personalized medicine. Genome Med. 2012;4:27.

12. Jin G, Wong STC. Toward better drug repositioning: Prioritizing and integrating existing methods into efficient pipelines. Drug Discov. Today. 2014;19:637–644.

13. Oprea TI, Nielsen SK, Ursu O, Yang JJ, Taboureau O, Mathias S, *et al*. Associating drugs, targets, clinical outcomes into an integrated network affords a new platform for computer-aided drug repurposing. Mol Inf. 2011;30:100–11.

14. Oprea TI. Virtual screening in lead discovery: a viewpoint. Molecules. 2002;7:51–62.

15. Seibert K, Zhang Y, Leahy K, Hauser S, Masferrer J, Perkins W, *et al*. Pharmacological and biochemical demonstration of the role of cyclooxygenase 2 in in?ammation and pain. ProcNatlAcadSci USA. 1994;91:12013–7.

16. Kurumbail RG, Stevens AM, Gierse JK, Mcdonald JJ, Stegeman RA, Pak JA, *et al*. Structural basis for selective inhibition of cyclooxygenase-2 by anti-in? ammatory agents. Nature. 1996;384:644–8.

17. Warner TD, Giuliano F, Vojnovic I, Bukasa A, Mitchell JA, Vane JR. Nonsteroid drug selectivities for cyclo-oxygenase-1 rather than cyclo-oxygenase-2 are associated with human gastrointestinal toxicity: a full in vitro analysis. Proc Natl Acad Sci USA. 1999;96:7563–8.

18. Celebrex® (celecoxib) capsules package information, http:// dailymed.nlm.nih.gov/dailymed/lookup.cfm?setid=8d52185d421f-4e34-8db7-f7676db2a226

19. Merck & Co., Inc. Merck announces voluntary worldwide withdrawal of Vioxx® (press release) Whitehouse Station, NJ, 2004.

20. Da Silva GMS, Lima LM, Fraga CAM, Sant'Anna CMR, Barreiro EJ. The molecular basis for coxib inhibition of p38a MAP kinase.Bioorg Med Chem Lett. 2005;15:3506–9.

21. Weber W, Casini A, Heine A, Kuhn D, Supuran CT, Scozzafava A, *et*

al. Unexpected nanomolar inhibition of carbonic anhydrase by COX-2-selective celecoxib: new pharmacological opportunities due to related binding site recognition. J Med Chem. 2004;47:550–7.

22. Mestres J, Gregori-Puigjané E, Valverde S, Solé RV. Data completeness—the Achilles heel of drug-target networks. Nat Biotechnol. 2008;26:983–4.

23. Campillos M, Kuhn M, Gavin AC, Jensen LJ, Bork P. Drug target identi?cation using side-effect similarity. Science. 2008;321:263–6.

24. Keiser MJ, Setola V, Irwin JJ, Laggner C, Abbas AI, Hufeisen SJ, *et al*. Predicting new molecular targets for known drugs. Nature. 2009;462:175–81.

25. Wermuth CG. The 'SOSA' approach: an alternative to highthroughput screening. Med Chem Res. 2001;10:431–9.

26. Mestres J, Gregori-Puigjané E, Valverde S, Solé RV. The topology of drug-target interaction networks: implicit dependence on drug properties and target families. Mol Bio Syst. 2009;5:1051–7.

27. Briansó F, Carrascosa MC, Oprea TI, Mestres J. Cross-pharmacology analysis of G protein-coupled receptors. Curr Top Med Chem. 2011;11:1956–63.

28. Collins FS. Mining for therapeutic gold. Nature Rev Drug Discov. 2011;10:397.

29. Lipworth WL, Kerridge IH, Day RO. Wrong questions, wrong answers? Are we getting the drugs we need? Clin Pharmacol Ther. 2012;91:367–9.

30. Prinz F, Schlange T, Asadullah K. Believe it or not: how much can we rely on published data on potential drug targets? Nat Rev Drug Discov. 2011;10:712–3.

31. Kinnings SL, Xie L, Fung KH, Jackson RM, Xie L, Bourne PE. The Mycobacterium tuberculosis drugome and its poly pharmacological implications. PLoSComput Biol. 2010;6:e1000976.

32. Shigemizu D, Hu Z, Hung JH, Huang CL, Wang Y, Delisi C. Using functional signatures to identify repositioned drugs for breast, myelogenous leukemia and prostate cancer. PLoSComput Biol. 2012;8:e1002347.

Chapter - 2
Common Methods used in Computational Protein Design

Authors

Bondeepa Saikia
Ph.D. Research Scholar, Department of Chemistry, Dibrugarh University, Dibrugarh, Assam, India

Aziza Rahman
Ph.D. Research Scholar, Department of Chemistry, Dibrugarh University, Dibrugarh, Assam, India

Soniya Agarwal
Ph.D. Research Scholar, Department of Chemistry, Dibrugarh University, Dibrugarh, Assam, India

Chapter - 2

Common Methods used in Computational Protein Design

Bondeepa Saikia, Aziza Rahman and Soniya Agarwal

Abstract

Proteins are the workhorses of living organisms. They are made up of amino acids linked together by peptide bond. A wide number of proteins can be found in nature that exhibit specific functions in their three dimensional folded states. They achieve their functional native structures through some selected pathways in biologically relevant time scale. The enormous and intricate interactions that are responsible for protein stability play vital role in protein folding. Computational protein design is an emerging field in protein biophysics that helps to understand the kinetics, thermodynamics and behavior of proteins. In protein design, sequences that fit the target structure are searched in the sequence space. The de novo protein design, protein re-engineering are the most studied area in computational protein design. In the last two decades many researchers and scientists have developed novel methods and strategies to study protein's thermodynamics, kinetics and behavior that are marked to be an important contribution to the field of computational protein design. With the advancement of computer hardware, knowledge of protein folding pathways, sequence and conformational sampling algorithms etc. it has become a lot easier to understand some of the behaviors and properties of proteins which were thought to be not possible two decades ago. Here, an introduction to computational protein design, common methods used in this field will be discussed and conclude with a brief outlook for the future.

Keywords: Protein, computational protein design

Abbreviation used: CPD (Computational protein design), GMEC (global minimum energy conformation)

1. Introduction

Proteins are very important biomolecule of living organisms. They are made up of amino acids which are covalently linked together by peptide bonds. There are twenty different amino acids commonly found in protein.

Protein structure can be classified into four categories- primary, secondary, tertiary and quaternary. The information regarding the three dimensional structure of a protein can be obtained from the sequence and hence the function of the protein. The experimental proof of this sequence-structure-function paradigm was first given by Christian Anfinsen and his colleagues in the 1950's [1]. This led to the generality *'Thermodynamic Hypothesis'* or *'Anfinsen Dogma'* which states that the protein's three-dimensional structure is the one which has the lowest Gibb's free energy in physiological conditions. This means in a given environment the native structure is determined by the interatomic interactions and hence by the amino acid sequence. This dogma says that the native structure is unique, stable and kinetically accessible minimum of the free energy [2].

A protein folds from its unfolded chain to a state which is functional and this state is known as protein native or folded state [3]. In protein biophysics, protein structure prediction or simply protein folding and protein design or inverse folding are the two fields that are mostly studied. In protein structure prediction, the structure of a protein is tried to predict from the information gained from amino acid sequence. On the contrary, in protein design the sequences that best fit a given target structure are searched in the sequence space. The compatible protein sequences are the sequences that have the minimum folding free energy. The process of designing sequences from a given three-dimensional structure to fulfill the urge of achieving new protein molecule with novel activity, the de novo design or re-engineer an existing protein to advance its activity and behavior is called the protein design. As we are saying we design sequences that fits the target structure, but it's not that easy. Consider a protein with sequence length 100. As there are 20 naturally occurring amino acids available, each residue site of the protein can be mutated 20 times with the 20 different amino acid each at a time. This means that we can have total 20^{100} amino acid sequences. This is the possible sequence space which is astronomically huge. Again, if we consider each amino acid of that protein chain prefers 3 different rotamers at its position, then 3^{100} different conformations are possible for the protein with 100 amino acid residues. This indicates that the conformation space is also very huge. This clearly shows the complexity of protein design problem. This vast sequence space and also the possible huge conformational space lead to various challenges that a protein designer has to face. Designing proteins with sophisticated computational methods helps to understand the physical principles underlying protein stability, folding kinetics, protein functional capability etc.

There are many diseases such as Alzheimer disease, Parkinson disease etc. which are caused by dysfunction of proteins due protein misfolding, protein aggregation. Since proteins are associated with many neurodegenerative diseases, research works that are focused on the cause of these diseases and finding their cure are need of the hour. With the help of computational protein design we can introduce novel activity by using de novo design, improve and enhance functional activity of existing proteins by redesigning them. These abilities to design functional proteins will lead to new routes for improved health care through innovative drugs, more efficient disease diagnostics. Moreover, computational protein design is offering the opportunity to unlock the potentially unlimited structural and functional space that is not sampled by nature.

2. Methods for computational protein design

In context of sequence-structure compatibility, a number of important advances in algorithms and theories related to protein folding and design have been developed in the recent years. In protein design the goal of these methods is to determine sequences that fold to a predetermined structure. These methods can be categorized in two types:

a) Methods considering the protein in atomistic detail

b) Methods that use reduced descriptions of the amino acid residues and backbone

In these methods, the protein backbone is kept fixed or slight variability is allowed. These methods of sequence design vary the amino acid sequences, aiming to optimize a given foldability criterion for a given target structure. Since enormous numbers of different sequences are possible for even a small protein, these methods must search the sequence space in a directed manner which does not consider every possible sequence or set of side-chain conformations [4]. Atomistic methods treat each protein sequence in full molecular detail. The goal of these methods is to understand and model the motion of each atom in the protein. Energy is calculated using an atom-based molecular potential derived from small molecule data. These methods minimize energy by varying sequence and side-chain conformation and they are performed remarkably well for small proteins. Since large protein will have more number of atoms and hence complexity in modeling the large protein will greatly increase and in that case these methods becomes more difficult to be carried out. However, sampling and elimination methods can be used to deal with large protein molecules [5]. In contrast to atomistic methods, methods with reduced description of amino acid residues do not consider all degrees of freedom of a protein. They reduce the

complexities applying some simplifications. The energy potentials used are mostly knowledge based: derived from database of known protein structure. The energy parameters used in these simplified potential are obtained statistically from the frequencies with which amino acid residues appear in a specific conformational environment [6, 7] or with which particular contacts present among the folded states [8, 9]. These simplified potentials allow for large variation in sequence and as well as structure. For example, lattice models are a class of these methods in which simplification is twofold: first, each of the residue is considered as a bead or a point in the lattice; second is each bead is restricted to be placed on the vertex of the lattice and to guarantee the chain connectivity, the amino acid residues that are linked in protein chain are placed on adjacent lattice vertex. Moreover, steric constraint is expressed by imposing the restriction that no more than one residue can occupy the same lattice vertex.

3. Algorithms: Sequence and conformational sampling methods

CPD use some optimization algorithms, also known as search algorithms which compute and give the best sequence and structure, expected to stabilize the target fold, in sequence and conformational space defined by biophysical input model. Biophysical model defines the sequence and conformational search space, the optimization objective (e.g., single state, multi-state, ensemble-based, etc.), and the energy function that scores for protein energetics [10]. Computational methods are helpful in determining optimal sequences; given the huge sequence space, methods that can search sequences likely to be fit into the target structure accelerate the discovery of new proteins. Searching global minimum energy conformation (GMEC) is a combinatorial problem of the sequence and discrete rotameric states for a given fold. However, it is the case that sequences having low sequence identity also have identical structure. This fact indicates that divergent sequences can also be used for some target fold and due to this fact; the sequence search problem in sequence space for protein design is a local minimization problem rather global. On the other hand, the conformational search problem is a global minimization problem, because, the native structural ensemble, in most cases, settles to the lowest free energy state [11]. The algorithms used for sequence and conformational sampling can be classified into two categories: Deterministic and stochastic and they are discussed in the sections below.

3.1 Deterministic algorithms

If a simulation model contains only deterministic (i.e., nonrandom) components, it is called deterministic. Deterministic algorithms, also called

as pruning algorithms [12], are designed to be similar to a systematic and exhaustive search of the sequence and conformational space. Due to complexity in searching exponentially large space of solution, deterministic algorithms start by simplifying the space of solution to a subset of the whole solution space and then rejection criteria are applied to identify the rotameric isomer that cannot be a member of the GMEC and thus eliminate that combinatorial possibilities [12]. If the algorithm runs to completion and finds a minimum energy conformation, these algorithms guarantee that it is the optimal solution for the design problem. These are usually empirically slower than stochastic algorithms. One advantage of these algorithms is that they provide a signaling mechanism on the complexity of the input model, if the results of these algorithms are unable to perform experimentally as predicted, then the error can be identified and is said to occur due to incorrect input biophysical model [10].

3.1.1 Dead-end-elimination algorithm

The Dead-End Elimination (DEE) theorem is based on a mathematical expression, called as the DEE criterion or elimination criterion, which is an iterative screening tool for rotameric isomers that cannot be present in the GMEC. Such rotamers are termed as "dead ending" and it is because any further combination with other rotamers will certainly results a global conformation, different from the minimum energy structure. This algorithm seeks to systematically eliminate bad rotamers or the dead ends and combinations of rotamers until a single solution is obtained. The iterative application of this criterion leads to a quasi-exponential decrease of the logarithm of conformational space as a function of the iteration cycles[13]. The theoretical basis of DEE proves that if DEE converges, the solution is the GMEC with no uncertainty [14]. This algorithm searches for the GMEC of a user-defined set of rotatable side chains, the template having rigid structure and the potential energy function used for calculation of potential energy of a protein in a given conformation is comprising of at most two-body interactions as given in the section of energy function i.e. energy description must be pairwise [15]. DEE algorithm either converges to the GMEC or it acts as a pre-filtering algorithm to reduce the search space so that the remaining search space can be searched by other algorithms. The fundamental theoretical concept of DEE can be stated as: if we consider two rotamers, i_r and i_t for amino acid residue i and j_s is a member of the set of all rotamers of other amino acid residues,S excluding amino acid residue i, then the rotamer i_r at residue i can be eliminated, which is incompatible with the GMEC, if the following inequality holds true:[13,15]

$$E(i_r) + \sum_{j}^{N} min_s E(i_r, j_s) > E(i_t) + \sum_{j}^{N} max_s E(i_t, j_s);\ i \neq j$$

The function $E(i_r)$ denotes one-body interaction plus template's self-energy, called the inherent energy of a rotamer. $E(i_r, j_s)$ is two-body interaction energy between two rotamers. The process is repeated iteratively until no rotamer states may be eliminated, and remaining rotamer configuration identifies the GMEC. The above single rotamer elimination method is extended to double-rotamer elimination, called the extended dead-end-elimination (EDEE). This involves a similar inequality to be satisfied and leads to the doubles elimination of the pair of rotamers i_r and j_s : [15]

$$\varepsilon(i_r, j_s) + \sum_{i,j \neq k}^{N} min_t \varepsilon(i_r, j_s, k_t) > \varepsilon(i_u, j_v) + \sum_{i,j \neq k}^{N} max_t \varepsilon(i_u, j_v, k_t)$$

Where, ε is the combined energy of rotamer pairs.

$$\varepsilon(i_r, j_s) = E(i_r) + E(j_s) + E(i_r, j_s)$$

$$\varepsilon(i_r, j_s, k_t) = E(i_r, k_t) + E(j_s, k_t)$$

There has been so much advancements in this algorithm, such extensions include Goldstein criterion [16], generalized criterion [17], split DEE criterion, split flags criterion [18] etc. These methods yield primarily information about sequences near or at the global optimum for a particular backbone structure. Due to large size of proteins, there is an exponential increase in computation time; this restricts DEE algorithms to be satisfactorily used for large proteins. However, they are often satisfactorily applied to small proteins with limited number of amino acid residues.

3.1.2 Self consistent mean field algorithm

Self consistent mean field algorithm (SCMF) is based on mean field theory approximation (MFT). Unlike DEE, SCMF is not guaranteed to converge on the optimal solution, the GMEC. However, it is deterministic; it converges to the same solution every time given the same initial conditions. SCMF uses mean-field description of the rotamer interactions to alter the energy landscape and advantage of using SCMF is that the computational time scales linearly with the number of residues instead of exponentially [19]. It is faster but less accurate than DEE and is generally used in situations where the protein of interest is too large for the problem to be tractable by DEE. In the protein, each monomer site experiences a distinct local environment determined by the target structure. The effective average energy

(field) at each site is determined self-consistently as the overall energy is lowered. Like DEE, this method explores conformational space by discretizing the dihedral angles of each side chain into a set of rotamers for each position in the protein sequence. This method iteratively develops a probabilistic description of the relative population of each possible rotamer at each position, and the probability of a given structure is defined as a function of the probabilities of its individual rotamer components. This method is significantly better at identifying correct side chain conformations in the protein's core than it is on identifying correct conformations of the surface and boundary amino acid side chains. As derived by Koehl and Delarue (1994), the mean-field energy for the rotamer i_r at residue i is given by:

$$E_{mf}(i_r) = E(i_r) + \sum_{j=1, j\neq i}^{N} \sum_{s=1}^{K_j} E(i_r, j_s) V(j_s)$$

Where, K_j represents the total number of rotamers at amino acid residue j; $V(j_s)$, called the conformational probability vector, represents site-specific probabilities of the rotameric states at amino acid residue j: the weight of each rotamer; the first term of the above relation denotes one-body interaction energy resulting from side chain-backbone interactions and the second term denotes the two body interaction energy resulting from rotamer-rotamer interactions. The conformational probability vector is normalized to unity:

$$\sum_{s=1}^{K} V(j_s) = 1$$

and it can be determined independently using following equation:

$$V(j_s) = \frac{e^{-\beta E_{mf}(j_s)}}{q_j}$$

$$V(j_s) = \frac{e^{-\beta E_{mf}(j_s)}}{\sum_{s=1}^{K_j} e^{-\beta E_{mf}(j_s)}}$$

where q_j is the partition function. The aim of this procedure is to make the mean-field energy landscape smooth and rendering the existence of multiple local minima; hence making it easier and simple to identify and locate the minimum of the mean-field energy landscape. The process is initialized with a uniform probability distribution of 1/Kj over the rotamers and uses annealing method to minimize the mean-field energy by selecting a

high initial temperature, often >20,000 K. Again, to implement a ceiling to which higher energies are set, a pair-energy threshold is used and for each side chain placement test case the optimal threshold is determined individually which is found to vary in the range 5-500 K Cal/mol. After the initialization step, mean-field energies for the amino acid residue and rotamer concerned are calculated. These are then converted to probabilities. To attain self-consistency and energy convergency, iteration is applied[19].

3.2 Stochastic algorithms

A model with at least one random input variable is called a stochastic model. Stochastic algorithms are relatively fast than deterministic algorithms but they are not guaranteed to find the GMEC with accuracy. They do not aim at rigorous search of GMEC instead they search the solution space randomly. They carry a random walk through the sequence and conformational space, and if they find a solution and this solution is accepted or rejected and then the algorithm moves to find another solution. In this way the lowest energy conformation found is taken as an approximate solution to the protein design problem [20]. If the algorithm fails to perform experimentally as predicted, the cause behind this failure of the protein design process cannot be known, if it is due to some error in the algorithm or in the input biophysical model.

3.2.1 Monte-Carlo: simulated annealing algorithm

Monte-Carlo: simulated annealing algorithm Monte Carlo algorithm is the simplest stochastic method that is widely used for sequence optimization. One important aspect of Monte Carlo methods is the ability to introduce a temperature factor with the search process which defines the degree to which sequences having high energy i.e. sequences with low foldability are accessible during the course of the search. This effective temperature is in consonance with statistical ideas concerning sequence evolution. Monte Carlo method involves random selection of rotamers of any amino acids followed by substitution of any one rotamer at a randomly selected amino acid position in the protein sequence. After the mutation, the energy of the new configuration, E_{new} is calculated and also the Boltzmann probabilities are calculated from the energy of the old configuration, E_{old} and new configuration, E_{new}. Metropolis Monte-Carlo [21] criteria is used to accept the move with a probability:

$$P = 1, if\ E_{new} < E_{old}\ and$$

$$P = e^{-\beta(E_{new}-E_{old})} if\ E_{new} > E_{old}$$

Where, $= \frac{1}{k_B T}$, is the Boltzmann constant and T is the temperature. The role of the temperature T is to overcome multiple local minima in the energy landscape. The way to rapidly explore the energy landscape is to start the process at a high initial temperature and gradually reducing the temperature to lower value. The temperature is then cyclically raised and lowered over the course of the run between the given temperature range. The optimization can be run for any number of cycles, each cycle containing a number of mutation attempts will settle down in a local free energy minimum and for getting better results MC can be run for longer time so that the output comes as the GMEC. Starting MC at higher temperature facilitates the acceptance of the moves with high energy change with a significant probability [11]. This whole process is called as simulated annealing. Some moves may create steric clashes resulting huge free energy pulse and hence those moves will not have much acceptance probability even at high temperature. To overcome this problem, creative moves should be essentially developed. However, convergence to the GMEC is not guaranteed. For rugged energy surfaces, conventional MC methods may become trapped in local minima which impede the sampling of low energy sequences. So, many different extensions of MC method are developed that include Monte Carlo with the quenching step (MCQ)[15], bias Monte Carlo (BMC) [22, 23], Mean field bias Monte Carlo (MFBMC) [24], Monte Carlo with replica exchange (MCREM) and biased Monte Carlo with replica exchange (BMCREM) [25]. In MCQ, after final MC run, all possible rotamers of the amino acids for each residue in the solution is randomly mutated. The new rotamer is kept if it is lower in energy, otherwise it is rejected. This quench step assures that there are no any other rotamer mutations that improve the energy further. In biased MC (BMC), based on configuration-biased MC, instead of using configuration monomer types are used as the variable. Here, each trial moves are biased by a predetermined probability so as to make the moves more likely to be accepted. In mean field bias MC, predetermined trial probabilities associated with a particular sequence are used that are generated from self-consistent mean field theory. Both BMC and MFBMC provide efficient sampling and better determination of lowest energy sequence. In replica exchange methods, an ensemble of non-interacting replicas of the original system at different temperatures is taken which simulated independently and simultaneously. It is done such that there is always only one replica at a definite temperature. Pairs of replicas at neighboring temperatures are exchanged with a transition probability such that the Boltzmann distribution is at equilibrium. In protein design process, replica exchange methods are

used that helps in overcoming local barriers and improves effective sampling of the sequence.

3.2.2 Genetic algorithm

Genetic algorithms are based on similar concept that of simulated annealing, simulated annealing being loosely based on principles of statistical mechanics whereas genetic algorithms are based on principles of natural selection. This method finds the lowest energy sequences for the target structure by traversing the sequence space with random mutation and recombination. Genetic algorithm usually begins with many random sequences, that is followed by generation of group of sequences by random mutation at a specific rate and then calculation of free energies of the generated sequences and ranking according to their values. The next step is recombination that involves pairing of the lowest energy solutions and then new mutations are applied for the next cycle. The advantage of this algorithm over Monte Carlo is that the population dynamics can overcome higher energy barriers by using larger moves than that used in MC. Genetic algorithms use biologically inspired operators in optimizing a population of solutions. A typical implementation involves encoding the variables, to be optimized, as a string of binary digits to generate a population of random strings. The next step is followed by subjecting this population to the genetic operators of selection, mutation, and crossover. The probability of a string surviving from one generation to the next relates to its fitness, where a fit string is a string relating to an optimal value of the target function. There are two ways by which each string may be randomly changed. The mutation operator simply selects a random bit in the string and changes it to a random value. Alternatively, using crossover operator to generate new strings that involves a randomly selected portion of one string is exchanged with a similar portion from another member of the string population [26].

4. Conclusion

The success and accuracy of a CPD depends largely on the biophysical model and therefore, it is of high need to improve this model. However, an improvement of these models relies on overcoming exponentially increased computational complexity of the sequence and conformational search problem. Since, simultaneous grow for computational hardware cannot be achieved at the same rate, the only practical solution to search more complex biophysical models is through novel algorithms. Till date there are no such theoretical and computational tools to design any protein structure or any protein-protein interface on demand. But it is important to remember that a

few years ago the idea of protein design was considered as an impossible task. Successful CPD depends on accurate structure modeling, ensuring protein stability, use of effective energy functions and optimizing inter-molecular interactions. But with advancement of computational techniques and new ideas, the pioneering group in CPD had achieved much already and has shown the way for many emerging researchers to realize the challenges and also the benefits and importance of this field. It is the fact that more researches must be carried on to solve the challenges in CPD which can have a great impact on improving health. Bold new steps are needed in integrating CPD methods, experimental screening protocols and structure identification techniques to achieve new milestones in CPD.

References

1. Sela M, White Jr FH, Anfinsen CB. Reductive cleavage of disulfide bridges in ribonuclease. Science. 1957;125(3250):691-692.
2. Anfinsen CB. Principles that govern the folding of protein chains. Science. 1973;181(4096):223- 230.
3. Dobson CM, Šali A, Karplus M. Protein folding: a perspective from theory and experiment. Angewandte Chemie International Edition. 1998;37(7):868-893.
4. Saven JG. Designing protein energy landscapes. Chemical reviews. 2001;101(10):3113–3130
5. Biswas P, Zou J, Saven JG. Statistical theory for protein ensembles with designed energy landscapes. The Journal of chemical physics. 2005;123(15):154908.
6. Miyazawa S, Jernigan RL. Estimation of effective inter residue contact energies from protein crystal structures: quasi-chemical approximation. Macromolecules. 1985;18(3):534–552.
7. Miyazawa S, Jernigan RL. Residue–residue potentials with a favorable contact pair term and an unfavorable high packing density term, for simulation and threading. Journal of molecular biology. 1996;256(3):623–644.
8. Goldstein RA, Luthey-Schulten ZA, Wolynes PG. Protein tertiary structure recognition using optimized Hamiltonians with local interactions. Proceedings of the National Academy of Sciences. 1992;89(19):9029–9033.

9. Mirny LA, Shakhnovich EI. How to derive a protein folding potential? A new approach to an old problem. Journal of molecular biology. 1996;264(5):1164–1179.

10. Gainza P, Nisonoff HM, Donald BR. Algorithms for protein design. Current opinion in structural biology. 2016;39:16–26.

11. Tian P. Computational protein design, from single domain soluble proteins to membrane proteins. Chemical Society Reviews. 2010;39(6):2071–2082.

12. Desjarlais JR, Clarke ND. Computer search algorithms in protein modification and design. Current opinion in structural biology. 1998;8(4):471–475.

13. Kenneth JM, LeGrand SM. The protein folding problem and tertiary structure prediction. 1st ed. Springer Science & Business Media; 2012.

14. Desmet J, De Maeyer M, Hazes B, Lasters I. The dead-end elimination theorem and its use in protein side-chain positioning. Nature. 1992;356(6369):539-542.

15. Voigt CA, Gordon DB, Mayo SL. Trading accuracy for speed: A quantitative comparison of search algorithms in protein sequence design. Journal of molecular biology. 2000;299(3):789–803.

16. Goldstein RF. Efficient rotamer elimination applied to protein side-chains and related spin glasses. Biophysical journal. 1994;66(5):1335–1340.

17. Looger LL, Dwyer MA, Smith JJ, Hellinga HW. Computational design of receptor and sensor proteins with novel functions. Nature. 2003;423(6936):185-190.

18. Gordon DB, Hom GK, Mayo SL, Pierce NA. Exact rotamer optimization for protein design. Journal of computational chemistry. 2003;24(2):232–243.

19. Koehl P, Delarue M. Application of a self-consistent mean field theory to predict protein side-chains conformation and estimate their conformational entropy. Journal of molecular biology. 1994;239(2):249–275.

20. Suárez M, Jaramillo A. Challenges in the computational design of proteins. Journal of the Royal Society Interface. 2009;6(suppl_4):S477–S491.

21. Metropolis N, Rosenbluth AW, Rosenbluth MN, Teller AH, Teller E. Equation of state calculations by fast computing machines. The journal of chemical physics. 1953;21(6):1087–1092.

22. Ferguson DM, Siepmann JI, Truhlar DG. Monte Carlo Methods in Chemical Physics. Wiley-Interscience, 1999.

23. Cootes AP, Curmi PM, Torda AE. Biased Monte Carlo optimization of protein sequences. The Journal of Chemical Physics. 2000;113(6):2489-2496.

24. Zou J, Saven JG. Using self-consistent fields to bias Monte Carlo methods with applications to designing and sampling protein sequences. The Journal of chemical physics. 2003;118(8):3843–3854.

25. Yang X, Saven JG. Computational methods for protein design and protein sequence variability: biased Monte Carlo and replica exchange. Chemical physics letters. 2005;401(1-3):205– 210.

26. Jones DT. De novo protein design using pairwise potentials and a genetic algorithm. Protein Science. 1994;3(4):567–574.

Chapter - 3
Electrochemical Treatment of Wastewater

Authors

Israfil Alam Tito
Applied Chemistry and Chemical Engineering, Noakhali Science and Technology University, Noakhali, Bangladesh

Md Rakib Hassan
Applied Chemistry and Chemical Engineering, Noakhali Science and Technology University, Noakhali, Bangladesh

Farhana Yasmin
Applied Chemistry and Chemical Engineering, Noakhali Science and Technology University, Noakhali, Bangladesh

Snahasish Bhowmik
Assistant Professor, Applied Chemistry and Chemical Engineering, Noakhali Science and Technology University, Noakhali, Bangladesh

Chapter - 3

Electrochemical Treatment of Wastewater

Israfil Alam Tito, Md Rakib Hassan, Farhana Yasmin and Snahasish Bhowmik

Abstract

Nowadays, purification of industrial effluents is a burning issue due to the continuous contamination of water by the effluents of various industries. There are many methods available for wastewater treatment. Among these, electrochemical treatment of wastewater has been extensively used over the last two decades due to its considerable separation performance. However, the operating cost of electrochemical treatment is high compared to other chemical and biological methods of water purification. In this chapter, we will discuss the various electrochemical techniques of waste water treatment, including their merits and demerits.

Keywords: Effluents, electrochemistry, separation, wastewater.

1. Introduction

Water has been an indispensable part of our daily life and its use has increased at twice the rate of population growth over the previous century. However, the effects of climate change are decreasing the supply of freshwater [1]. Wastewater from various sources contains suspended and dissolved solids such as heavy metals, pesticides, fertilizers, organic waste, etc. [2]. The concentration of these pollutants is increasing in the freshwater resources due to industrial and municipal wastewater discharge, decreased runoff, reduced water dilution capacity, and agricultural intensification. They are also responsible for the emissions of GHG [3, 4]. It is estimated that the demand for freshwater will be increased by 55% globally between 2000 and 2050 [5]. Only 8% of municipal and industrial wastewater is treated, and more than 80% of wastewater is released into the environment without proper treatment, causing various health and environmental impacts, including increased GHG emissions, water temperature, and decreased industrial and agricultural production along with biodiversity [6-8]. To overcome these impacts, wastewater treatment has become very important to us. Wastewater treatment and collection systems are mainly of two types: (a) Offsite system, where the wastewater source is from a sewerage network,

and (b) On-site system, where wastewater is collected in a septic tank and opened in another location. Common effluent treatment plants are used in wastewater treatment for small and medium-sized businesses but with less efficiency in comparison to the electrochemical process [9, 10].

Electrochemical technology is used in the treatment of wastewater. Although this method of wastewater treatment is costly, it has remarkable efficiency over other conventional methods. The efficiency and cleanliness of the products from this method are enhanced by both membrane and biological processes [11, 12]. In this chapter, we will briefly describe the general principle of electrochemical treatment of waste water and various kinds of electrochemical treatments with their pros and cons.

2. Principle of electrochemical treatment of waste water

The electrochemical process is a physico-electrochemical method and a branch of physical chemistry. It plays an important role in industrial wastewater treatment, where it deals with the transfer of charge between electrodes and pollutants to oxidize the pollutants. An electricity source is used to supply the electrons into the wastewater via electrodes. This process involves a considerable number of electrodes. The organic pollutants are directly or indirectly oxidized by the electrodes, or they could be reduced by the cathodes. Anode produces a lot of hydroxyl radical and reactive oxygen species. Those radical oxidized organic pollutants make carbon dioxide and water. From this reaction, different types of gases are produced, such as oxygen, hydrogen, chlorine, nitrogen, carbon dioxide, etc. Those gases also bring the pollutants upward. So, in the electrochemical process of wastewater, anything can happen, such as mineralization of pollutants, reduction and oxidization of pollutants, and the evolution of different kinds of gases.

2.1 Mechanism of the electrochemical mineralization

In general, oxygen is transferred from water to the reaction products during anodic oxidation processes. This is known as EOTR. An example of EOTR is the electrochemical mineralization of acetic acid where oxygen atoms are obtained from water for the oxidation of acetic acid to CO_2. However, water must be activated in order to achieve the EOTR. There are two possible ways for the electrochemical activation of water in acid media depending on the electrode material: (1) by dissociative water adsorption in the potential region of water's thermodynamic stability and (2) by electrolysis of water at potentials greater than its thermodynamic stability [13].

a) Activation of water by dissociative adsorption

In acid media, water is adsorbed on the electrode, which discharges hydrogen, resulting in the formation of chemisorbed hydroxyl radicals on the anode surface.

$H_2O + E \rightarrow E - OH + E{-}H$ …… (i)

$E{-}H \rightarrow E + H^+ + e^-$……..… (ii)

$H_2O + E \rightarrow E - OH + H^+ + e^-$…… (iii)

The reaction takes place at an anode potential which is lower than the thermodynamic potential of 1.23 V/SHE, under standard conditions. The bonding energy of E–OH and E–H exceeds the dissociation energy of water to H• + HO• at the electrode (E) on which the dissociative adsorption of water can be obtained. According to the Langmuir–Hinshelwood mechanism, the EOTR occurs at the electrode surface, where both the organic molecule and the hydroxyl radicals are adsorbed. This method is suitable for fuel cell applications but limited to simple C1 organic molecules such as methanol or formic acid. Furthermore, due to CO chemisorption on the electrode active sites, there are problems associated with electrode deactivation.

Due to the lack of active electrocatalytic anode material, it is not feasible to produce electrical energy simultaneously with the electrochemical mineralization of organic pollutants. To overcome this problem, a new active field in the development of bio-fuel cells has recently been demonstrated named Bio-electrocatalysis [13].

b) Activation of water by electrolytic discharge

In acid media, water is discharged on the electrode at a thermodynamic potential of 1.23 V/SHE, under standard conditions, producing hydroxyl radicals, which are the O_2 evolution reaction intermediates.

$H_2O + E \rightarrow E(^{\bullet}OH) + H^+ + e^-$……. (iv)

$E(\bullet OH) \rightarrow E + \frac{1}{2} O_2 + H^+ + e^-$……..…… (v)

The reactivity of electrolytic hydroxyl radicals and chemisorbed hydroxyl radicals is very different. If we do not know the nature of the interactions between the hydroxyl radicals (electrolytically generated) and the electrode surface (E), we consider these hydroxyl radicals as physisorbed on the anode surface. The EOTR between an organic compound P and the hydroxyl radicals takes place close to the anode's surface:

$P_{(aq)} + E\ (\bullet OH)_{n/2} \rightarrow E + \text{Oxidation products} + n/2\ H^+ + n/2\ e^-$……(vi)

Here, n= number of electrons involved in the oxidation reaction of P [13].

3. Classification of electrochemical treatment

Electrochemical treatment can be classified into various types, such as-

1) Direct Anodic Oxidation.
2) Indirect Electrochemical Oxidation.
3) Electro Fenton Process.
4) Electrochemical Floatation.
5) Solar-Driven Photo-Electro-Fenton Process.
6) Electrochemical Deposition.
7) Electrochemical Coagulation.

We will describe each process followed by its advantages and disadvantages.

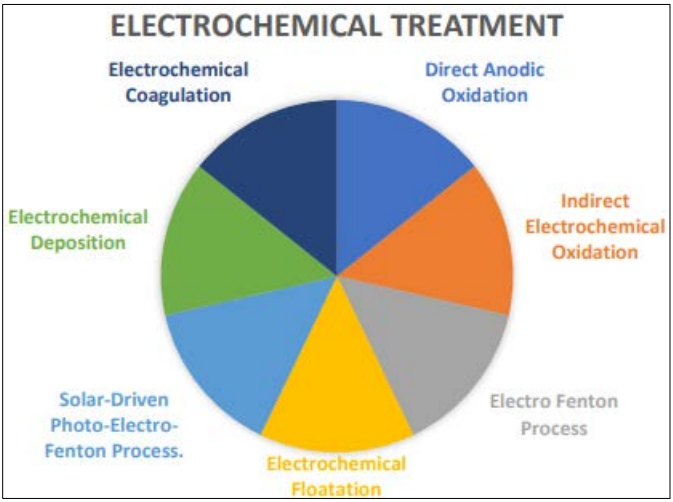

3.1 Direct anodic oxidation

Direct anodic oxidation is a process where pollutants are oxidized after adsorbing at the anode. In this process, electrons are exchanged by pollutants from the anode surface without any involvement of other substance [14, 15]. It consists of two steps. Firstly, pollutants are diffused from the bulk solution to the anode surface for adsorption. Secondly, oxidation of pollutants occurred at the anode surface [16]. Figure 1 illustrates the process of direct anodic oxidation where pollutants can be oxidized by physically adsorbed

"active oxygen" (adsorbed hydroxyl radicals, •OH) (eq iii), or can be oxidized by chemically adsorbed "active oxygen" (oxygen in the oxide lattice, MOx+1) (eq iv). Active oxygen (physical) can cause the complete combustion of organic compounds (R) (eq iii) or participate in the formation of selective oxidation products (chemical) (eq iv) [17]. The direct electrochemical oxidation rate depends on the catalytic activity of the anode, diffusion rate of pollutants, applied current density, and electrode types. Anode with low oxygen evolution overpotential shows "active" behavior. Whereas, anode with high oxygen evolution shows "non-active" behavior. The anode with low oxygen evolution overpotential exhibits selective oxidation of pollutants due to producing a huge amount of oxygen which impedes the contact between pollutants and anode. In wastewater treatment, an ideal electrode is one that causes complete electrochemical oxidation of organics to CO_2. SnO_2, PbO_2, and boron-doped diamond (BDD) are examples of such electrodes. Cotillas *et al.* studied the removal of procion Red MX-5B dye from wastewater using BBD anode and reported that initial dye content, and chemical oxygen demand (COD) were completely removed [18, 19, 20, 21].

$$2H_2O - 4e^- \rightarrow O_2 + 4H^+ \text{ ..... (i)}$$

$$H_2O + M \rightarrow M[OH\bullet] + H^+ + e- \text{ ..... (ii)}$$

$$R + MOx(\bullet OH)z = CO_2 + z\,H^+ + z\,e + MOx \text{ ..... (iii)}$$

$$R + MOx+1 = RO + MOx \text{ ..... (iv)}$$

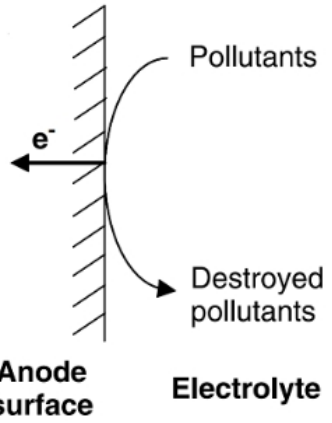

Fig 1: Direct anodic oxidation process [22].

Advantages

- Oxidation occurs without the involvement of other substances.

- Removal of color and organic substances are effective.
- Not required to add a large number of chemicals.

Disadvantages

- High operating cost.
- This process has fouling problem [14, 17, 23, 24].

3.2 Indirect electrochemical oxidation

Indirect electrochemical oxidation is a process where pollutants are oxidized by an electrode indirectly with the help of the in situ electrochemically generated highly oxidant species at the electrode surface [25, 26, 27]. Peroxide, Fenton's reagent, Cl_2, hypochlorite, peroxodisulfate, and ozone can all be utilized as oxidants to aid in the oxidation of pollutants at the electrode surface [28]. As a result, contaminants and oxidants interact in the bulk solution rather than at the electrode surface. Figure 2 illustrates the indirect electrochemical oxidation process and the rate of oxidation is affected by the rate of oxidant penetration into solution, temperature, and pH [29]. Among all the anodically generated oxidants for industrial wastewater treatment, active chlorine is the most traditional one and the most widely used. Therefore, we will discuss the indirect electrochemical generation of active chlorine which is initiated by converting chloride ions to chlorine with the help of the anode surface (eq i). The liberated chlorine reacts with water and produces hypochlorous acid (HOCl) (eq ii) which dissociates into OCl^- and H^+ ions in the bulk solution (Eq. iii). Hypochlorite ion, the principal oxidizing agent, reacts with organic pollutants by destroying them (eq iv) [30]. For indirect electrochemical oxidation, several different types of anodic materials are employed, however for active chlorine generation, platinum or a mixture of metal oxides such as RuO_2, TiO_2, and IrO_2 are used [31]. Vlyssides and Israilides studied electrochemical degradation of textile dye and finishing wastewater using a Ti/Pt anode and reported that after 40 min of electrolysis, there was 92% COD, 92.2% BOD, and 94% color reduction with energy consumption of 44 kWh/kg of COD removal [32].

$$2Cl^- \rightarrow Cl_2 + 2e^- \ldots\ldots\ldots\ldots\ldots\ldots \text{(i)}$$

$$Cl_2 + H_2O \rightarrow HOCl + H^+ + Cl^- \ldots\ldots. \text{(ii)}$$

$$HOCl \leftrightarrow H^+ + OCl^- \ldots\ldots\ldots\ldots\ldots \text{(iii)}$$

$$R + OCl^- \rightarrow CO_2 + H_2O + Cl^- \ldots\ldots\ldots \text{(iv)}$$

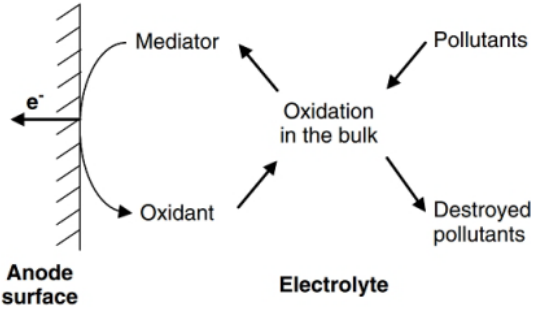

Fig 2: Indirect electrochemical oxidation process [33]

Advantages

- It can eliminate the fouling problem.
- Both inorganic and organic pollutants can be removed.
- Amenability to automation.
- Easy handling.

Disadvantages

- A number of side reactions occur which causes reduction in the process efficiency.
- If the chlorine content is low then an extra amount of salt is added for improving efficiency [30, 31].

3.3 Electro fenton process

The Electro-fenton is an advanced oxidation process (AOPs) where wastewater organic pollutants are oxidized by a highly reactive hydroxyl radical (·OH). The anodic material for EF is iron, and the cathodic materials include graphite, BDD, carbon nanotubes, activated carbon filters, gas-diffusion-electrode (GDE), etc. Fenton's reagents are H_2O_2 and Fe^{2+}, where H_2O_2 is produced by the reduction of O_2 with protons at the cathode (eq i) and Fe_2^+ is produced by the sacrificial iron anode (eq ii) [34, 35, 36]. A homogenous reaction between H_2O_2 and Fe^{2+} produces the active oxidizing agent (·OH) (eq iv). Although the reaction is slow, the oxidation of water produces an oxidizing agent (·OH) at the anode (eq iii) which reacts with organic pollutants and mineralization into CO_2 and water (eq v, vi). The reaction requires high currents, suitable electrode materials, and a low pH=3. If the pH is above four, ferric oxyhydroxides become precipitates (eq vii-ix), which can be dissolved by decreasing pH below 2.5. However, such pH maintenance makes the process much more difficult to continue [37, 38].

Figure 3 illustrates the Electro-Fenton process and the factors that affect this process are the effect of current density, the effect of pH, Fe^{2+} concentration, and the effect of flow rate [39, 40]

Cathode: $O_2 + 2e^- + 2H^+ \rightarrow H_2O_2$ ……..…… (i)

Sacrificial Anode: Fe - $2e^{-}$ $\rightarrow Fe^{2+}$ ……..……(ii)

$H_2O + \rightarrow \bullet OH + H^+ + e^-$ ……..……..…(iii)

$Fe^{2+} + H_2O_2 \rightarrow Fe^{3+} + \bullet OH + OH^-$ ……(iv)

• OH + Organic pollutant → Primary intermediates … (v)

Primary intermediates + • OH → → → $CO_2 + H_2O$ + inorganic ions (vi)

If pH of the solution increase

$Fe^{3+} + OH^- \Leftrightarrow Fe(OH)^{2+}$ ……(vii)

$Fe(HO)^{2+}$ + OH- $\Leftrightarrow Fe(OH)^{2+}$..……(viii)

$Fe(HO)^{2+}$ + OH- $\Leftrightarrow Fe(OH)_3$ ……(ix)

$Fe(OH)_3 + Fe(OH)_3 \Leftrightarrow$ precipitate..……(x)

$Fe(OH)_3$ + precipitate → precipitate …… (xi)

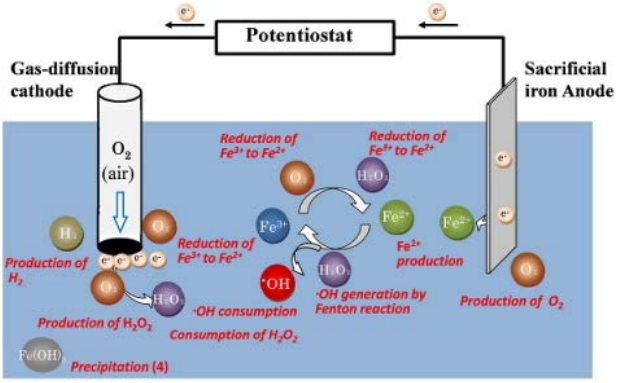

Fig 3: Electro-fenton process [34].

Advantages

- Simple process design
- Low installation cost
- Highly effective for removing COD and pollutants.
- Improve higher biodegradability of treated wastewater.
- Unnecessary storage of dangerous H_2O_2 is not required.

Disadvantages

- Low pH maintenance is difficult.
- High energy consumption [41, 42].

3.4 Electrochemical floatation

Electrochemical flotation is a process that produces tiny bubbles of hydrogen and oxygen gases for separating suspended particles or particles produced from other processes (e.g., electrocoagulation) in wastewater [43, 44]. During the electrochemical flotation (EF) process, the current is passed through the electrodes, where free atomic oxygen bubbles are evaluated in the diffusion layer of the anode (eq i) which penetrates into the wastewater and combines with pollutants [45]. Consequently, the cathode also produces hydrogen gases, and combines with pollutants (eq ii) illustrated in figure 4(b). Commonly used cathode materials include stainless steel, nickel, titanium, and anodic materials include graphite, PbO_2, Pt, etc. If the anodes are made of an active metal such as iron, metal cations are produced (eq iv, v, vi) [46, 47]. These cations act as coagulating agents. But the main difference between EC and EF is that the complex of coagulating agents and pollutants is removed afterward by EF [48]. Generally, electrodes are arranged at the bottom of the tank. When the pollutants are comes in contact with the surface, a skimmer is used for pollutants separation. Figure 4(a) illustrates the Electrochemical floatation process and the factors which affect this process are pH, current density, arrangement of the electrodes, etc. [49]. M. Belkacem *et al.* said that the EF process has an average removal efficiency of 93% and reported that, the kinetics of electrochemical flotation is fast and does not exceed 15 min (effectiveness = 95– 99%), except for nickel [50].

At the anode electrode: $2H_2O\ (l) \rightarrow O_2\ (g) + 4H^+\ (aq) + 4e^-$ …….... (i)

At the cathode electrode: $2H_2O + 2e^- \rightarrow H_2\ (g) + 2OH^-\ (aq)$ ……(ii)

Overall redux reaction: $2H_2O\ (l) \rightarrow 2\ H_2\ (g) + O_2\ (g)$..……. (iii)

Additional reaction

At anode: $Fe - 2\ e^- \rightarrow Fe^{2+}$ …… (iv)

At alkaline conditions: $Fe^{2+} + 2OH^- \rightarrow Fe(OH)_2$ …….. (v)

At acidic conditions: $4Fe^{2+} + O_2 + 2H_2O \rightarrow 4Fe^{3+} + 4OH^-$ ……..… (vi)

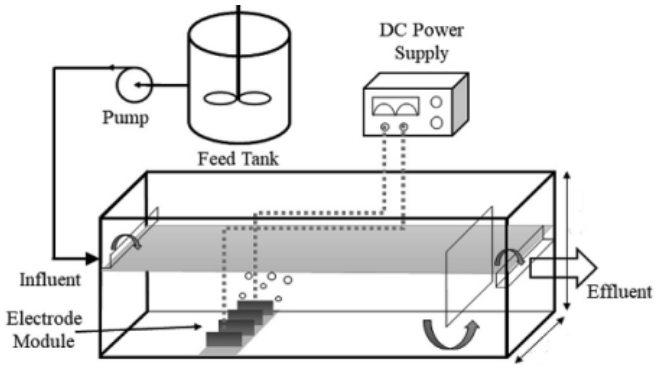

Fig 4(a): Electrochemical flotation process [43]

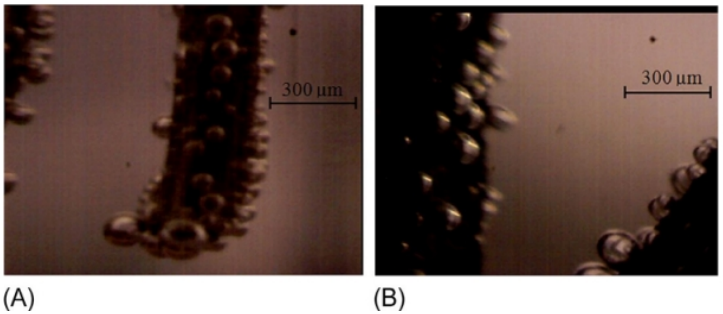

Fig 4(b): A is hydrogen bubbles at the cathode and B is oxygen bubbles at the anode [47]

Advantages

- Gas bubbles are finer and more uniform.
- The size and density of electrolytic bubbles can be controlled by electric current density.
- Specific separation can be designed by a specific electrode surface.
- Electrochemical flotation can be used without adding chemicals.
- Short process time.
- Absence of secondary pollution of water for insoluble electrodes.

Disadvantages

- Operating cost is primary concern in this process [51, 52, 53, 54].

3.5 Solar-driven photo-electro-fenton process (SPEF)

It is a combination process of solar irradiation and electrochemical fenton for the efficient elimination of organic pollutants. This combination

can be applied in two ways, firstly, direct solar treatment where solar energy is used directly for the photodegradation of pollutants in a photoreactor [55]. Secondly, indirect solar treatment, in which solar energy can be used indirectly to generate electricity for electrochemical cells. In the electro-fenton process, $Fe^{2+}$and H_2O_2 generates Fe^{3+} and •OH in the Fenton reaction under the acidic condition (eq i). The ferrous ion is regenerated by an electrochemical Fenton-based process (eq ii). In the SPEF process, •OH and UV radiation generated from sunlight under EF conditions and degradation is enhanced due to UV photons which increase the photoreduction of $Fe(OH)^{2+}$ to Fe^{2+} and •OH via reaction (eq iii) and the photolysis of Fe(III)-carboxylate products by reaction (eq iv) [56, 57, 58]. Figure 5 illustrates the process of SPEF and parameters for the degradation of organic compounds by Solar Photoelectro-Fenton Process are current density, the concentration of catalyst, organic concentration, and the solar radiation intensity, pH etc. [59]. E. Gil Pavas *et al.* said that at optimum operational conditions (pH = 4, j = 40 mA/cm^2, σ = 5768 μS/cm and Fe^{2+} = 0.3 mM) the solar-driven process let to obtain total discoloration, COD reduction of 83% and TOC mineralization of 70% after 15 min of electrolysis [60].

$$Fe^{2+} + H_2O_2 \rightarrow Fe^{3+} + \bullet OH + OH^- \quad \text{(i)}$$

$$Fe^{3+} + e^- \rightarrow Fe^{2+} \quad \text{(ii)}$$

$$Fe(OH)^{2+} + h\nu \rightarrow Fe^{2+} + \bullet OH \quad \text{(iii)}$$

$$Fe(OOCR)^{2+} + h\nu \rightarrow Fe^{2+} + CO_2 + R\bullet \quad \text{(iv)}$$

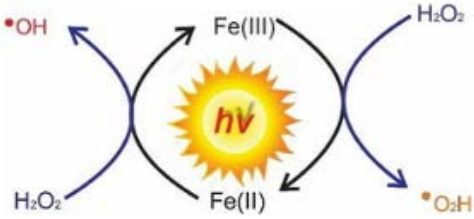

Fig 5: Reactions that occur when the fenton process is irradiated with UV [61]

Advantages

- SPEF is economical
- UV lamps are unnecessary.
- Reduces energy consumption.
- Use renewable energy source.
- Environment friendly

Disadvantages

- Sometimes SPEF reactors are difficult to scale up [59, 62].

3.6 Electrochemical deposition

Electrochemical deposition is an electrochemical process where heavy metals are removed from wastewater. When an electric current is applied to the electrochemical deposition process, the anode proceeds an oxidation reaction while the cathode proceeds a reduction reaction where positively charged metal cations are reduced by the cathode (eq i) [63, 64, 65]. However, the most frequent reaction is between the proton ions and the hydrogen gases (eq ii). The anode material should be selected correctly so that, the process proceeds properly. Anodes that are insoluble or inert are preferred. The common anodic reaction produces oxygen gas (eq iii). If the wastewater contains chelating agents like EDTA, NTA, and citrate, they additionally improve recovery efficiency as they produce stronger complexes with metal ions [66, 67]. Some reports say that the addition of sodium chloride distinctly increases the removal of heavy metals [68]. Factors affecting the electrodeposition process are current, pH, and conductivity [69]. A. Kuleyin *et al.* said that the copper ion removal for 60 min at pH 3 was 66% with the copper cathode and 80% with the stainless-steel cathode.

Cathodic reactions

$M^{n+}_{(aq)} + 2e^- \rightarrow M^0_{(s)}$ ..... (i)

$2H^+_{(aq)} + 2e^- \rightarrow H_{2(g)}$ ..... (ii)

Anodic reactions

$4OH^-_{(aq)} \rightarrow O_{2(g)} + 2H_2O + 4e^-$ ..... (iii)

Advantages

- The electrochemical deposition process is reagentless.
- It is highly selective.
- Low operating cost.
- This process sludge less product.

Disadvantages

- Sometimes this process produces loose or spongy deposits.
- Must be minimized hydrogen production reaction or the dioxygen reduction [63, 67, 70].

3.7 Electrochemical coagulation

Electrochemical coagulation is a technique where wastewater pollutants (suspended, emulsified, or dissolved) are destabilized by destabilizing agents. Generally, in the electrochemical coagulation process (Al or Fe), metal electrodes are frequently used [71, 72]. When an electric current is applied to wastewater, the anode material starts to produce metal cations (eq i) and water undergoes a hydrolysis reaction to generate hydroxyl ions at the cathode (eq iii). Metal cations and hydroxyl ions are then combines to form metal hydroxides, also called destabilizing agents, which have tremendous adsorption ability to bind the pollutants and react with pollutants to make neutralized matter, then starts to aggregate and adsorb on metal hydroxides, where most of them are precipitates. As we see that in eq (ii and iii), oxygen and hydrogen gases are produced and a number of pollutants are going upwards as flotation [73, 74, 75, 76]. The process of electrochemical coagulation illustrates in figure 6. The factors that affect electrochemical stability are pH, pollutant type and concentration, bubble size and position, floc stability, and agglomerate size [77]. Saravanan *et al.* concluded that removal efficiency of 91% COD under 3 A/dm^2 of current density, pH of 6.5, and 2 g/L electrolyte concentration [78].

Anode: $M \rightarrow M^{n+} + ne^-$ …… (i)

$H_2O \rightarrow 4H^+ (aq) + O_2 (g) + 4e^-$……(ii)

Cathode : $2H_2O + 2e^- \rightarrow H_2 + 2OH^-$ …… (iii)

Overall : $M^{n+} + nH_2O \rightarrow nH^+ + M(OH)n$

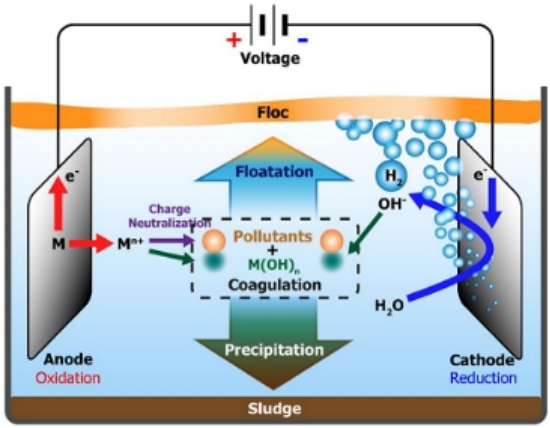

Fig 6: Electrochemical coagulation process [79]

Advantages

- Simple equipped and easy to operate.
- No external use of chemicals.
- Less sludge generation.
- Small colloidal particles also settle.
- EC treated wastewater well pleasant, odorless, clear and colorless water.

Disadvantages

- Regular change of electrodes and maintenance.
- Oxide layer formation on electrode surface leads to passivation of the electrode.
- Conductivity of wastewater.
- The electricity may not be easily available and expensive in some areas [80, 81, 82].

Conclusion

Electrochemical treatments have been explored frequently over last decades as an industrial effluent treatment process. In this chapter, seven types of electrochemical techniques are outlined. Although chlorinated intermediates are formed during the indirect oxidation of pollutants of industries, it is being used for the treatment of effluents of biorefractory industries. In addition, direct anodic oxidation is considered one of the easiest technologies in the separation of pollutant from wastewater. Then, Electroflotation is frequently used for the treatment of effluents of mining industries. Besides, it has been found that electrocoagulation has showed superior performances in treating industrial effluents containing suspended solids, oil and grease, and even organic or inorganic pollutants. And, electro fenton process, solar-driven photo-electro-fenton process and electrochemical deposition are also potential strategies for the separation of pollutants from waste water. Finally, it is essential to develop hybrid technology in order to implement highly efficient electrochemical technology for the treatment of industrial effluents.

References

1. Envi Stats India report. Envi Stats India 2018 (Supplement on Environmental Accounts). Gov. India, Minist. Stat. Program. Implement, 2018, 1-249. http://www.mospi.gov.in/sites/default/files/reports_and_publications/statistical_publication/EnviStats_Inda_27sep18.pdf. 16 March, 2021.

2. WWAP (United Nations World Water Assessment Programme). The United Nations World Water Development Report 2017: Wastewater, The Untapped Resource. Paris, UNESCO, 2017.

3. Saravanan A, Kumar PS, Varjani SJ, Suresh K. Effective removal of Cr(VI) ions from synthetic solution using Mixed Biomasses: Kinetic, Equilibrium and Thermodynamic study. Journal of Water Process Engineering. 2021;40(3):101905.

4. Varjani SJ, Sudha MC. Water Remediation. Springe, Singapore. 2018;1(1):91-115.

5. Organization for economic co-operation and development. OECD Environmental outlook to 2050: the consequence of Inaction. Paris, OECD Publishing, 2012. www.oecdlibrary.org/docserver/9789264122246en.pdf?expires=1576513787&id=id&accname=ocid177643&checksum=ESD1E6D4DB78962941DAA08F2B58D805. 16 March 2021.

6. Khanal SK, Varjani S, SKL C, Awasthi K. Waste-to-resources: Opportunities and Challenges. Bioresour Technol. 2020;317:123987.

7. WWDR Report, WWDR-2020. Journal of Chemical Information and Modeling, 2020.

8. Shah AV, Srivastava VK, Mohanty SS, Varjani S. Municipal solid waste as a sustainable resource for energy production: State-of-the-art review. Journal of Environmental Chemical Engineering. 2021;9(3):105717.

9. Varjani SJ, Gnansounou E, Pandey A. Comprehensive review on toxicity waste and their degradation by microorganisms. Chemosphere. 2017;188:280-291.

10. Report CETP. Global good practices in industrial wastewater treatment and disposal/reuse with special reference to common effluent treatment plants. 2016;60:1-66.

11. Liu Y, Deng YY, Zhang Q, Liu H. Overview of recent developments of resource recovery from wastewater via electrochemistry-based technologies. Science of Total Environment. 2021;757(7):143901.

12. Perera ML, Englehardt JD, Dvorak AC. Technologies for recovering nutrients from wastewater: a critical review. Environmental Engineering Science. 2019;36(5):511-529.

13. Kapalka A. Foti G, Comninellis C. Electrochemistry for the Environment Springer, 2010, 1-23.

14. Feng Y, Yang L, Liu J, Logan BE. Electrochemical technologies for wastewater treatment and resource reclamation. Environ. Sci. Water Res. Technol. 2016;2(5):800-831.

15. Suman H, Sangal VK, Vashishtha M. Treatment of tannery industry effluent by electrochemical methods: A review. Mater Today Proc. 2021;47:1438-1444.

16. Drogui P, Blais JF, Mercier G. Review of Electrochemical Technologies for Environmental Applications. Recent Patents Eng. 2008;1(3):257-272.

17. Chen G. Electrochemical technologies in wastewater treatment. Sep. Purif. Technol. 2004;38(1):11-41.

18. Martínez-Huitle CA, Panizza M. Electrochemical oxidation of organic pollutants for wastewater treatment. Curr. Opin. Electrochem. 2018;11:62-71.

19. Martínez-Huitle CA, Ferro S. Electrochemical oxidation of organic pollutants for the wastewater treatment: Direct and indirect processes. Chem. Soc. Rev. 2006;35(12):1324-1340.

20. Panizza M, Cerisola G. Direct and mediated anodic oxidation of organic pollutants. Chem. Rev. 2009;109(12):6541-6569.

21. Sirés I, Brillas E, Oturan MA, Rodrigo MA, Panizza M. Electrochemical advanced oxidation processes: Today and tomorrow. A review. Environ. Sci. Pollut. Res. 2014;21(14):8336-8367.

22. Anglada Á, Urtiaga A, Ortiz I. Contributions of electrochemical oxidation to waste-water treatment: Fundamentals and review of applications. J. Chem. Technol. Biotechnol. 2009;84(12):1747-1755.

23. Yang Chu Y, Jing Wang W, Wang M. Anodic oxidation process for the degradation of 2, 4-dichlorophenol in aqueous solution and the enhancement of biodegradability. J. Hazard. Mater. 2010;180(1-3):247-252.

24. Hamad H, Bassyouni D, El-Ashtoukhy ES, Amin N, Abd El-Latif M. Electrocatalytic degradation and minimization of specific energy consumption of synthetic azo dye from wastewater by anodic oxidation process with an emphasis on enhancing economic efficiency and reaction mechanism. Ecotoxicol. Environ. Saf. 2017;148:501-512.

25. Garcia-Segura S, Ocon JD, Chong MN. Electrochemical oxidation remediation of real wastewater effluents - A review. Process Saf. Environ. Prot. 2018;113:48-67.

26. Morsi MS, Al-Sarawy AA, El-Dein WAS. Electrochemical degradation of some organic dyes by electrochemical oxidation on a pb/pbo2 electrode. Desalin. Water Treat. 2011;26(1-3):301-308.

27. Singh S, Lo SL, Srivastava VC, Hiwarkar AD. Comparative study of electrochemical oxidation for dye degradation: Parametric optimization and mechanism identification. J. Environ. Chem. Eng. 2016;4(3):2911-2921.

28. Jüttner K, Galla U, Schmieder H. Electrochemical approaches to environmental problems in the process industry. Electrochim. Acta. 2000; 45(15-20):2575-2594.

29. Anthuvan Babu S, Raja S, Sibi S, Neeraja P. Decolorization of synthetic and real polluted water by indirect electrochemical oxidation process. Pollut. Res. 2012;31(1):45-49.

30. Bassyouni DG, Hamad HA, El-Ashtoukhy ESZ, Amin NK, El-Latif MMA. Comparative performance of anodic oxidation and electrocoagulation as clean processes for electrocatalytic degradation of diazo dye Acid Brown 14 in aqueous medium. J. Hazard. Mater. 2017;335:178-187.

31. Martínez-Huitle CA, Panizza M. Electrochemical oxidation of organic pollutants for wastewater treatment. Curr. Opin. Electrochem. 2018;11:62-71.

32. Vlyssides AG. Israilides CJ. Electrochemical oxidation of a textile dye and finishing wastewater using a Pt/Ti electrode. J. Environ. Sci. Heal. - Part A Toxic/Hazardous Subst. Environ. Eng. 1998;33(5):847-862.

33. Anglada Á, Urtiaga A, Ortiz I. Contributions of electrochemical oxidation to waste-water treatment: Fundamentals and review of applications. J. Chem. Technol. Biotechnol. 2009;84(12):1747-1755.

34. Kubo D, Kawase Y. SC. J. Clean. Prod, 2018.

35. Cheng-Chun J, Jia-fa Z. Progress and prospect in electro-Fenton process for wastewater treatment. Journal of Zhejiang University. 2007;8(7):1118-1125.

36. Gümüs D. Comparison of Fenton and electro-Fenton processes for oxidation of phenol. 2016;3(3):252-258.

37. Oturan N, MA Oturanand Applications. Elsevier Inc., 2018.

38. He H, Zhou Z. Technology Electro-Fenton process for water and wastewater treatment. Crit. Rev. Environ. Sci. Technol. 2017;0(0):1-32.

39. Ma L, Zhou M, Ren G, Yang W, Liang L. A highly energy-efficient flow-through electro-Fenton process for organic pollutants degradation. Electrochim. Acta, 2016.

40. Kushwaha PKVKSJP. Parametric study of electro - Fenton treatment for real textile wastewater, disposal study, and its cost analysis. Int. J. Environ. Sci. Technol, 2018.

41. Anisah S, Lun W, Wahab A. Journal of Water Process Engineering Electro-Fenton technology for wastewater treatment: A bibliometric analysis of current research trends, future perspectives and energy consumption analysis. J. Water Process Eng. 2021;40(40):101952.

42. Sirés I, Brillas E, Oturan MA, Rodrigo MA, Panizza M. Electrochemical Advanced Oxidation Processes: Today and Tomorrow. Anelectrochemical advanced oxidation processes:today and tomorrow. A review Organic compound, July, 2014.

43. Mohtashami R, Shang JQ. Treatment of automotive paint wastewater in continuous-flow electroflotation reactor. J. Clean. Prod. 2019;218:335-346.

44. Selim KA, El Hosiny FI, Khalek MAA, Osama I. Kinetics and Thermodynamics of Some Heavy Metals Removal from Industrial Effluents Through Electro-Flotation Process. Colloid Surf. Sci. 2017;2(211):47-53.

45. Priya PG. Degradation Studies of Tannery Effluents using Electro Flotation Technique. J. Chem. Eng. Process Technol. 2011;2(1):2-5.

46. Matis KA, Peleka EN. Alternative flotation techniques for wastewater treatment: Focus on electroflotation. Sep. Sci. Technol. 2010;45(16):2465-2474.

47. Santiago Santos GO, Salles Pupo MM, Vasconcelos VM, Barrios Eguiluz KI, Salazar Banda GR, Electroflotation. 2018.

48. Mook WT, Aroua MK, Issabayeva G. Prospective applications of renewable energy based electrochemical systems in wastewater treatment: A review. Renew. Sustain. Energy Rev. 2014;38:36-46.

49. Chen G, Hung YT. Electrochemical Wastewater Treatment Processes. Adv. Physicochem. Treat. Technol. 2007;5:57-106.

50. Belkacem M, Khodir M, Abdelkrim S. Treatment characteristics of textile wastewater and removal of heavy metals using the electroflotation technique. Desalination. 2008;228(1-3):245-254.

51. Mohtashami R, Shang JQ. Electroflotation for Treatment of Industrial Wastewaters: A Focused Review. Environ. Process. 2019;(2):325-353.

52. Alam R, Shang JQ. Electrochemical model of electro-flotation. J. Water Process Eng. 2016;12:78-88.

53. Muddemann T, Haupt D, Sievers M, Kunz U. Electrochemical Reactors for Wastewater Treatment. Chem. Bio. Eng. Rev. 2019;6(5):142-156.

54. Kolesnikov VA, Il'in VI, Kolesnikov AV. Electroflotation in Wastewater Treatment from Oil Products, Dyes, Surfactants, Ligands, and Biological Pollutants: A Review. Theor. Found. Chem. Eng. 2019;53(2):251-273.

55. Bugueño-Carrasco S, Monteil H, Toledo-Neira C, Sandoval MÁ, Thiam A, Salazar R *et al*. Elimination of pharmaceutical pollutants by solar photoelectro-Fenton process in a pilot plant. Environ. Sci. Pollut. Res. 2021;28(19):23753-23766.

56. Salazar R, Arriaza JG, Vidal J, Vera CR, Neira CT, Sandoval MA *et al.* Treatment of industrial textile wastewater by the solar photoelectro-Fenton process: Influence of solar radiation and applied current. Sol. Energy. 2019;190:82-91.

57. Olvera-Vargas H, Oturan N, Oturan MA, Brillas E. Electro-Fenton and solar photoelectro-Fenton treatments of the pharmaceutical ranitidine in pre-pilot flow plant scale.n Sep. Purif. Technol. 2015;146:127-135.

58. Gozzi F, Sirés I, Thiam A, de Oliveira SC, Junior AM, Brillas E *et al*. Treatment of single and mixed pesticide formulations by solar photoelectro-Fenton using a flow plant. Chem. Eng. J. 2017;310:503-513.

59. Gutierrez-Mata AG, Martinez SV, Gallegos AA, Ahmadi M, Perez JAH, Ghanbari F *et al*. Recent Overview of Solar Photocatalysis and Solar Photo-Fenton Processes for Wastewater Treatment. Int. J. Photoenergy, 2017.

60. GilPavas E, Dobrosz-Gómez I, Gómez-García MÁ. Optimization of solar-driven photo-electro-Fenton process for the treatment of textile industrial wastewater. J. Water Process Eng. 2018;24:49-55.

61. Peralta-Hernández JM, Vijay S, Rodríguez-Narváez O, Pacheco-Álvarez

MA. Photo and solar fenton processes for wastewater treatment. Electrochem. Water Wastewater Treat, 2018, 223-237.

62. Vidal J, Carvajal A, Huiliñir C, Salazar R. Slaughterhouse wastewater treatment by a combined anaerobic digestion/solar photoelectro-Fenton process performed in semicontinuous operation. Chem. Eng. J. 2019;378:122097.

63. Widiyanto H, Kosimaningrum WE, Rahmayetty. Electrodeposition for rapid recovery of cobalt (II) in industrial wastewater. IOP Conf. Ser. Earth Environ. Sci. 2021;623(1):12054.

64. Feng Y, Yang L, Liu J, Logan BE. Electrochemical technologies for wastewater treatment and resource reclamation. Environ. Sci. Water Res. Technol. 2016;2(5):800-831.

65. Dean JG, Bosqui FL, Lanouette KH. Removing heavy metals from waste water. Environ. Sci. Technol. 1972;6(6):518-522.

66. Azimi A, Azari A, Rezakazemi M, Ansarpour M. Removal of Heavy Metals from Industrial Wastewaters: A Review. Chem. BioEng. Rev. 2017;4(1):37-59.

67. Kuleyin A, Uysal HE. Recovery of copper ions from industrial wastewater by electrodeposition. Int. J. Electrochem. Sci. 2020;15(2):1474-1485.

68. Hefny RA, Abdel-Salam OE, Basstawesy AM, Mahmoud MH, Barakat NAM. Fast and efficient removal of iron from industrial wastewater using electrochemical deposition. Int. J. Electrochem. Sci. 2019;14(9):9369-9379.

69. Chen X, Lin H, Ren HY, Xing JL. Experimental study on wastewater treatment containing copper with electrodeposition method. Adv. Mater. Res. 2013;779:1670-1673.

70. Tomkiewicz M. Environmental Aspects of Electrodeposition. Mod. Electroplat. 2011;5:555-571.

71. Abbas SH, Ali WH. Electrocoagulation Technique Used To Treat Wastewater: A Review. Am. J. Eng. Res. 2018;7(10):74-88.

72. Bharath M, Krishna BM, MKB. A Review of Electrocoagulation Process for Wastewater Treatment. Int. J. Chem. Tech. Res. 2018;11(3):289-302.

73. Zaied BK, Rashid M, Nasrullah M, Zularisam AW, Pant D, Singh L *et*

al. A comprehensive review on contaminants removal from pharmaceutical wastewater by electrocoagulation process. Sci. Total Environ. 2020;726:138095.

74. Syam Babu D, Anantha Singh TS, Nidheesh PV, Suresh Kumar M. Industrial wastewater treatment by electrocoagulation process. Sep. Sci. Technol. 2020;55(17):3195-3227.

75. Lekhlif B, Oudrhiri L, Zidane F, Drogui P, Blais JF. Study of the electrocoagulation of electroplating industry wastewaters charged by nickel (II) and chromium (VI). J. Mater. Environ. Sci. 2014;5(1):111-120.

76. Naje AS, Chelliapan S, Zakaria Z, Ajeel MA, Alaba PA. A review of electrocoagulation technology for the treatment of textile wastewater. Rev. Chem. Eng. 2017;33(3):263-292.

77. SMDU Islam. Electrocoagulation (EC) technology for wastewater treatment and pollutants removal. Sustain. Water Resour. Manag. 2019;5(1):359-380.

78. Butler E, Hung YT, Yeh RYL, Al Ahmad MS. Electrocoagulation in wastewater treatment. Water (Switzerland). 2011;3(2):495-525.

79. An C, Huang G, Yao Y, Zhao S. Emerging usage of electrocoagulation technology for oil removal from wastewater: A review. Sci. Total Environ. 2017;579:537-556.

80. Guevara HM, Roy S. Waste Water Recycling and Management, Springer, Singapore, 2019.

81. Crini G, Lichtfouse E. Advantages and disadvantages of techniques used for wastewater treatment. Environ. Chem. Lett. 2019;17(1):145-155.

82. Demirhan E. Response surface methodology approach for adsorptive removal of Reactive Blue 19 onto green pea pod. Water Sci. Technol. 2020;81(6):1137-1147.

Chapter - 4
Radon, Thoron and Gamma Dose Rate in Different Flooring Materials of Dwellings in an Urban Environment of Bengaluru

Author

Sathish LA

Department of Physics, Government Science College, Bengaluru, Karnataka, India

Chapter - 4

Radon, Thoron and Gamma Dose Rate in Different Flooring Materials of Dwellings in an Urban Environment of Bengaluru

Sathish LA

Abstract

The measurements of Radon, Thoron and gamma dose was carried out inside dwellings of different flooring materials. The objective of the study was to understand the contribution of building construction materials towards Radon, Thoron and gamma dose levels in indoor environments. It was observed that the Granite floorings had higher dosage levels than mosaic floorings, which had lower dose levels and this may be attributed to higher exhalation of Radon gas from Granite samples than that of mosaic samples. The detailed experimental results are discussed in the present research work.

Keywords: Gamma dose, Radon, Thoron, flooring type, Bengaluru

Introduction

The naturally occurring radioactive elements ^{238}U, ^{232}Th, and their short-lived progenies, as well as singly occurring radio nuclides like ^{40}K and ^{87}Rb, contribute significantly to background radiation levels in the earth's crust. These properties have given the study of Health Physics, Radiation Physics, and related fields of Physics a new perspective to study its effects. Ionizing radiation is continually present in nature, which exposes humans to it. The assessment of radiation doses to humans from natural radioactive sources is particularly important because these sources account for the majority of the global dose absorbed [1]. Natural background radiation levels vary just slightly in most parts of the world. Scientific, industrial, and technical activity may cause natural radiation levels to increase modestly. The two types of naturally occurring radio nuclides are those that occur individually and those that come from one of the three radioactive decay series: ^{238}U, ^{232}Th, or Actinium. As illustrated in figure 1, ^{238}U and ^{232}Th, as well as their daughters, produce the majority of natural ionizing radiation [2].

The main sources of artificial radionuclides are past atmospheric nuclear

weapon tests, nuclear accidents, and nuclear power reactor operation. Because of their longer half-lives, the radionuclides ^{90}Sr ($T_{1/2}$ = 28.8 years) and ^{137}Cs ($T_{1/2}$ = 30.2 years) produced by nuclear explosions contribute significantly to the health hazard. ^{90}Sr, which is chemically similar to calcium, enters the human body via the calcium pathway and accumulates in the skeleton, resulting in internal exposure. The ^{137}Cs is chemically similar to potassium and follows its path, after entering the human body and is distributed relatively uniform in soft tissues [3].

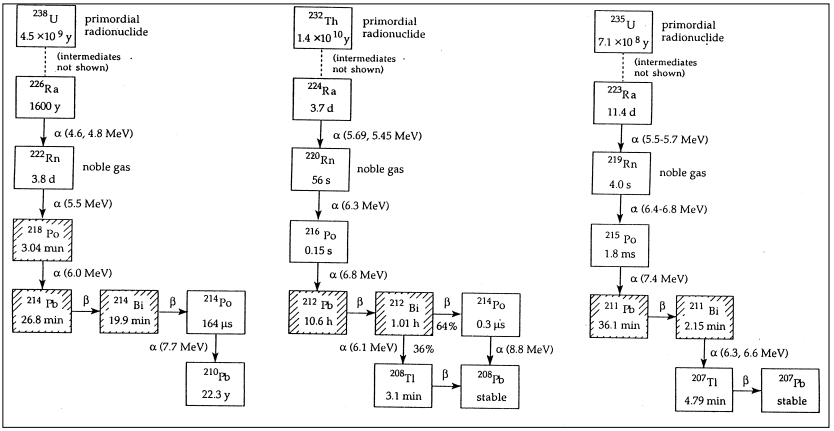

Fig 1: The decay chain of Uranium and Thorium (Nazaroff, 1992)

The main sources of ^{238}U and its daughter products in surface air are re suspension of soil dust from the earth's crust, release of fly-ash from coal-fired power plants, mining, milling, and processing of Uranium ore, disposal of nuclear waste from nuclear power plants, oil refineries, fallout re suspension from past atmospheric nuclear weapon detonations, satellite and other nuclear-related accidents, and industrial activities such as phosphate fertilizer manufacturing [4]. When ^{226}Ra enters the body, it behaves similarly to calcium in terms of metabolism, with a significant portion of it being deposited in bone. More than 70% of ^{226}Ra in the body is concentrated in bone, with the remainder distributed rather evenly across the body's soft tissues [1]. With the production of alpha-particles, the radioactive noble gas ^{226}Ra found in the earth's crust decays to ^{222}Rn, a radioactive noble gas with a half-life of 3.82 days. The ^{222}Rn atoms escape from the soil and enter the atmosphere through diffusion mechanisms.

Recoil of the ^{222}Rn atoms during the decay of ^{226}Ra is assumed to be the primary cause of ^{222}Rn atoms escaping from soil particles into air-filled pores. ^{222}Rn must diffuse through the pores of the soil material to reach the free

atmosphere, and only a percentage of it will reach the surface before dying. Due to the complex diffusion path, some ^{222}Rn atoms will be expelled into the closed pores, where they will be trapped. Emanation describes the process of ^{222}Rn molecules diffusing from soil grains into pores. The concentration of ^{238}U, ^{232}Th and ^{40}K in the rock samples of different regions of India is given in table 1.

Table 1: Estimated ^{238}U, ^{232}Th and ^{40}K content in Indian rocks

State	^{238}U	^{232}Th	^{40}K	^{40}K (%)
	Bqkg^{-1}			
Andaman & Nicobar	31.5	27.4	378.2	1.22
Andhra Pradesh	33.2	40.9	511.5	1.65
Arunachal Pradesh	34.9	98.2	620.0	2.00
Assam	63.0	129.3	747.1	2.41
Bihar	40.9	36.9	502.2	1.62
Daman & Diu	55.7	24.5	412.3	1.63
Delhi	32.6	30.4	579.7	1.87
Goa	33.0	30.5	412.3	1.33
Gujarat	55.7	24.5	505.3	1.63
Haryana	32.6	30.4	579.7	1.87
Himachal Pradesh	32.6	30.4	579.7	1.87
Jammu & Kashmir	43.4	29.0	545.6	1.76
Karnataka	33.0	30.5	412.3	1.33
Kerala	45.1	47.6	558.0	1.80
Madhya Pradesh	44.0	31.6	458.8	1.48
Maharashtra	31.7	33.4	508.4	1.64
Manipur	95.2	36.2	505.3	1.63
Meghalaya	66.7	32.0	517.7	1.67
Mizoram	35.5	28.8	579.7	1.87
Nagaland	89.1	39.5	620.0	2.00
Orissa	35.4	110.3	499.1	1.61
Pondicherry	27.4	33.1	471.2	1.52
Punjab	32.6	30.4	579.7	1.87
Rajasthan	36.7	32.1	508.4	1.64
Tamil Nadu	27.4	33.1	471.2	1.52
Tripura	33.1	28.5	480.5	1.55
Uttar Pradesh	32.9	33.8	629.3	2.03
West Bengal	47.9	45.1	576.6	1.86

Radon can infiltrate the indoor environment through a variety of routes,

including diffusion through construction materials, soil breaches, and foundation fissures. A modest negative pressure difference (under pressure) between the indoor and external atmosphere causes radon to enter the indoor air at a higher rate. Wind blowing through the building and heating inside the building (cold nations) are two aspects that contribute to this (UNSCEAR, 1993). The pressure difference between the inside of the house and the soil causes radon infiltration from the ground into the house. The flow of radon into the house is enhanced if the air pressure inside the house is lower than the pressure in the soil. Temperature and pressure changes can cause a stack effect, which draws air into the house from the bottom. Water supplies usually contribute only a tiny amount to indoor radon levels, but they might be the primary source in locations where ground water ^{222}Rn levels are extremely high. Table 2 shows the Radon entrance rates for a model building in temperate climates [5].

Table 2: Radon entry rates for a model building

Sources of Radon	Mechanism	Entry rates ($Bqm^{-1}h^{-1}$)
Building elements	Diffusion	10
Subjacent earth	Diffusion	7.5
Outdoor air	Advection	20
Water supply	Infiltration	10
Natural gas	De-emanation	1
	Consumption	0.3

Important factors that influence the indoor radon concentrations are:

- The ^{222}Rn emission from the earth or building materials is dependent on the ^{226}Ra content, density, and porosity of the materials. ^{222}Rn enters the interior air through cracks and other openings.
- Because of the warm interior air, atmospheric pressure is frequently lower in homes than outside. The Stack effect provides a moderate suction at the ground level in an indoor environment. Under pressure can also be created by wind blowing across chimneys and windows.
- Building construction: The ventilation rate, which is controlled by the kind of building construction, usage of insulating materials, artificial ventilation systems, and other factors, affects the radon entry.
- Meteorological characteristics: The most essential parameters that affect both radon entrance rates and ventilation rates are air pressure, wind velocity, wind direction, and temperature.

Since research on Uranium miners discovered a positive risk coefficient for lung cancer in miners exposed to high amounts of ^{222}Rn and its progeny,

there has been a rise of interest in programs that assess ^{222}Rn in the environment. The discovery of increased ^{222}Rn levels in the indoor environment in many countries heightened interest in residential ^{222}Rn as a potential public health hazard in the Western world. A large-scale indoor ^{222}Rn and ^{220}Rn survey was also planned to lead to a quantitative understanding of the dosage effects of radon exposures, in conjunction with epidemiological investigations [1].

Hence, the measurements were carried out in different parts of Bengaluru metropolitan city limits, to understand the levels of indoor ^{222}Rn, ^{220}Rn, and their progenies in different floorings of dwellings.

Location of present study

The area of present study is Bangalore metropolitan, India and the locative map is shown in figure 2.

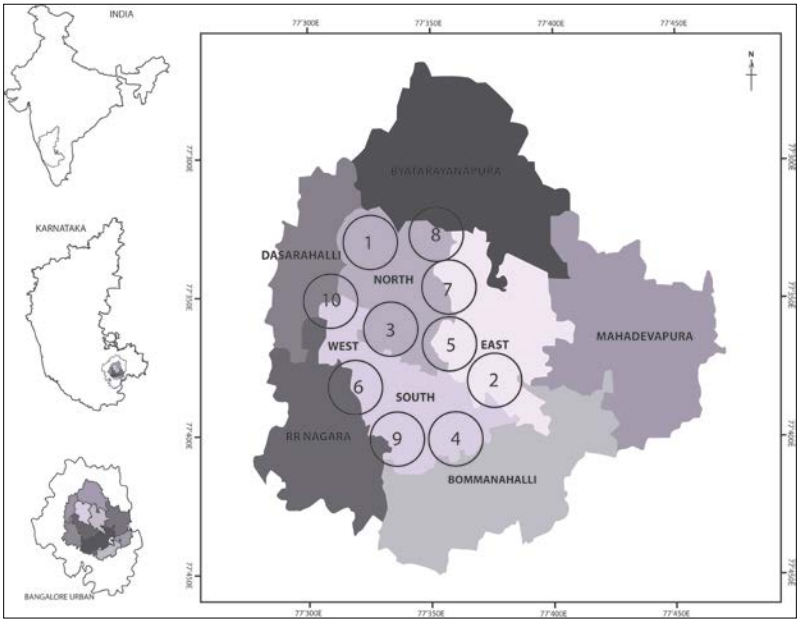

Fig 2: Locative map of Bangalore metropolitan, India

[Rajajinagar (RAJ) – 1, Jayanagar (JNR) – 2, Srirampuram (SRPM) – 3, Padhmanabhanagar (PNR) – 4, Gandhinagar (GNR) – 5, Srinivasanagar (SRN) – 6, Sheshadripuram (SHPM) - 7

Malleshwaram (MLM) – 8, Banashankari (BSK) – 9, Vijayanagar (VNR) – 10]

Summer is from March to May in Bengaluru, wet season is from June to September, post monsoon season is from October to November, and winter is from December to February. The hottest month is often April, with average daily maximum temperatures of 30-35 ^{0}C and average daily minimum temperatures of 20-24 ^{0}C. This region's geology is dominated by granite, with a diverse range of granites, granitic gneiss, pegmatite, and other minerals. The monitored homes were all on the ground floor. Around twenty houses of diverse architectural types were chosen in each of the observed locations.

Instrumentations Used

Solid State Nuclear Track Detectors

SSNTDs are dielectric thin sheets such as cellulose nitrate and polycarbonates that serve as insulators. They are susceptible to alpha but not to beta or gamma radiation. Small (3–10nm) damage tracks are left by a highly ionising alpha particle passing through such an insulating material. Chemical chains are disrupted, free radicals are produced, and other issues arise as a result of this damage. These damaged areas can dissolve at a far faster rate than the undamaged material when exposed to certain chemical agents known as etchants. The dissolved part is depicted as a track in the movie. The amount of such tracks determines how many alpha particles are produced. To make dosimeters, SSNTDs are employed. The dosimeter system consists of a two-component cylindrical plastic cup with a facility for maintaining a specific concentration of SSNTD films.

The films used in each of the three exposure settings are 2.5 cm × 2.5 cm. The dosimeter with the films described above was exposed for about 90 days during four quarters of the year. About 150 residences were randomly picked in Bangalore Metropolitan, India, with diverse features such as different types of flooring, rooms, walls, and rooms of various volumes to expose the dosimeters. The dosimeter cups were created, manufactured, and donated by the Bhabha Atomic Research Centre in Mumbai, India [6].

Low Level Radon Detection System (LLRDS)

This method was designed and developed by Srivastava 1994. After ^{222}Rn decays by alpha emission, around 90% of the decay result, RaA (^{218}Po) atoms, carry positive charge for a brief time. The charged state might last anywhere from seconds to minutes, depending on the environment. The fact that the daughter atom is charged is used to calculate the concentration. The LLRDS concept is shown in Figure 3.

A 5-litre cylindrical chamber serves as the sampling device. The chamber

measures 240mm in diameter and 115mm in height. It is made of aluminum and has a wall thickness of 3 mm. A swage lock quick connector is supplied, allowing either vacuum transfer or flow through sample extraction. The sample air enters and exits the chamber through this opening. A unique feature of this connector is that the valve opens when the male connector is inserted and closes instantly when the connector is removed.

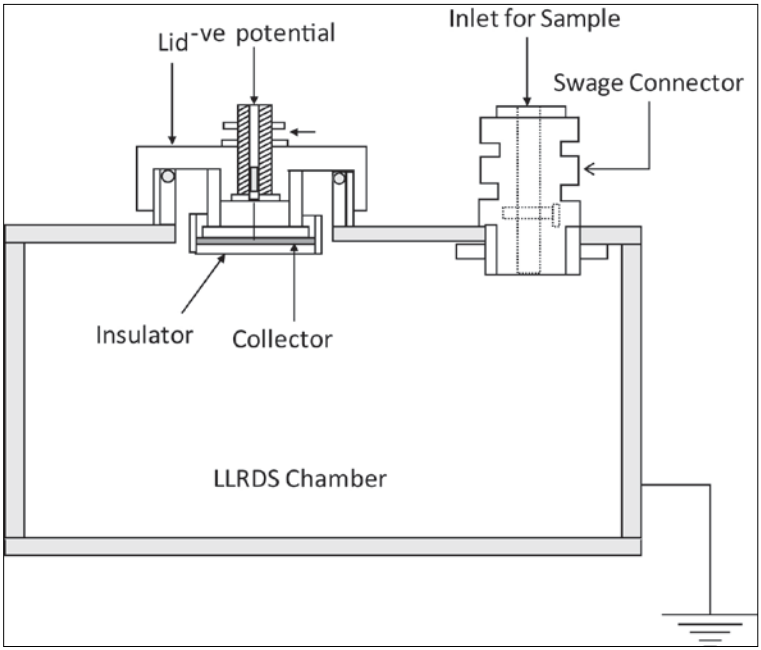

Fig 3: Schematic of LLRDS Chamber

A 60 mm diameter circular aperture at the top of the chamber that can be sealed with a cap and into which a charge plate is inserted. An insulated connector is located on the cap's outside side (BNC connector). The BNC connector is fixed on the Perspex holder by an aluminum plate (charge plate). The charge plate, which is protected from the chamber body, is kept in touch with the 5cm diameter metallic collecting disc utilized to collect ^{222}Rn progeny. The collection plate receives an external supply of –800 volts. The electrostatic field created attracts the RaA atoms within to the charged plate. The collection plate's potential of –800 volts was changed to match the chamber's requirements [7-8].

Results and Discussion

Variation of indoor ^{222}Rn, ^{220}Rn, their progeny levels along with the dose rates were measured for dwellings of different floorings at Srirampuram, wide

variations in the concentrations of ^{222}Rn, ^{220}Rn, their progeny and dose rates were observed and they were found to vary from 49.16 to 65.93 Bqm^{-3}, 6.18 to 18.54 Bqm^{-3}, 0.17 to 0.61 mWL, 0.039 to 0.041 mWL and 1.33 to 1.96 $mSvy^{-1}$, 40.94 to 45.19 Bqm^{-3}, 16.30 to 20.14 Bqm^{-3}, 0.14 to 0.18 mWL, 0.04 to 0.05 mWL and 1.29 to 1.46 $mSvy^{-1}$, 27.46 to 32.97 Bqm^{-3}, 20.60 to 28.85 Bqm^{-3}, 0.09 to 0.11 mWL, 0.045 to 0.063 mWL and 1.02 to 1.30 $mSvy^{-1}$, 10.99 to 16.96 Bqm^{-3}, 6.87 to 28.47 Bqm^{-3}, 0.06 to 1.16 mWL, 0.03 to 1.86 mWL and 0.38 to 0.89 $mSvy^{-1}$, 18.13 to 22.81 Bqm^{-3}, 8.33 to 29.17 Bqm^{-3}, 0.06 to 0.12 mWL, 0.018 to 0.065 mWL and 0.59 to 1.05 $mSvy^{-1}$ for granite flooring, concrete flooring, red oxide flooring, mosaic flooring and stone flooring respectively. Whereas the arithmetic mean concentrations of ^{222}Rn, ^{220}Rn, their progeny and dose rates for granite flooring, concrete, red oxide, mosaic flooring and stone flooring were 57.54, 12.36 Bqm^{-3}, 0.39, 0.040 mWL and 1.64 $mSvy^{-1}$, 43.06, 18.22 Bqm^{-3}, 0.16, 0.042 mWL and 1.38 $mSvy^{-1}$, 31.13, 25.76 Bqm^{-3}, 0.11, 0.056 mWL and 1.20 $mSvy^{-1}$, 13.67, 16.64 Bqm^{-3}, 0.51, 0.71 mWL and 0.61 $mSvy^{-1}$, 21.00, 18.98 Bqm^{-3}, 0.083, 0.046 mWL and 0.84 $mSvy^{-1}$ respectively.

Variation of indoor ^{222}Rn, ^{220}Rn, their progeny levels along with the dose rates were measured for dwellings of different floorings at Rajajinagar, wide variations in the concentrations of ^{222}Rn, ^{220}Rn, their progeny and dose rates were observed and they were found to vary between 49.16 to 65.93 Bqm^{-3}, 6.18 to 18.54 Bqm^{-3}, 0.17 to 0.61 mWL, 0.039 to 0.041 mWL and 1.33 to 1.96 $mSvy^{-1}$, 40.94 to 45.19 Bqm^{-3}, 16.30 to 20.14 Bqm^{-3}, 0.14 to 0.18 mWL, 0.041 to 0.044 mWL and 1.29 to 1.46 $mSvy^{-1}$, 27.46 to 32.97 Bqm^{-3}, 20.60 to 28.85 Bqm^{-3}, 0.09 to 0.11 mWL, 0.045 to 0.063 mWL and 1.02 to 1.30 $mSvy^{-1}$, 10.99 to 16.96 Bqm^{-3}, 6.87 to 28.47 Bqm^{-3}, 0.06 to 1.16 mWL, 0.03 to 1.86 mWL and 0.38 to 0.89 $mSvy^{-1}$, 18.13 to 22.81 Bqm^{-3}, 8.33 to 29.17 Bqm^{-3}, 0.065 to 0.121 mWL, 0.018 to 0.065 mWL and 0.59 to 1.05 $mSvy^{-1}$ for granite flooring, concrete flooring, red oxide flooring, mosaic flooring and stone flooring respectively. Whereas the arithmetic mean concentrations of ^{222}Rn, ^{220}Rn, their progeny and dose rates for granite flooring, concrete, red oxide, mosaic flooring and stone flooring were 57.54, 12.36 Bqm^{-3}, 0.39, 0.040 mWL and 1.64 $mSvy^{-1}$, 43.06, 18.22 Bqm^{-3}, 0.16, 0.042 mWL and 1.38 $mSvy^{-1}$, 31.13, 25.76 Bqm^{-3}, 0.11, 0.056 mWL and 1.20 $mSvy^{-1}$, 13.67, 16.64 Bqm^{-3}, 0.51, 0.71 mWL and 0.61 $mSvy^{-1}$, 21.00, 18.98 Bqm^{-3}, 0.083, 0.046 mWL and 0.84 $mSvy^{-1}$ respectively.

Variation of indoor ^{222}Rn, ^{220}Rn, their progeny levels along with the dose rates were measured for dwellings of different floorings at Vijayanagar, wide variations in the concentrations of ^{222}Rn, ^{220}Rn, their progeny and dose rates

were observed and they were found to vary from 87.33 to 99.42 Bqm^{-3}, 10.99 to 29.86 Bqm^{-3}, 0.33 to 1.04 mWL, 0.03 to 0.10 mWL and 2.37 to 2.98 $mSvy^{-1}$, 76.02 to 82.71 Bqm^{-3}, 20.83 to 34.72 Bqm^{-3}, 0.27 to 0.29 mWL, 0.05 to 0.08 mWL and 2.25 to 2.64 $mSvy^{-1}$, 50.29 to 57.89 Bqm^{-3}, 15.80 to 32.97 Bqm^{-3}, 0.18 to 0.37 mWL, 0.06 to 0.07 mWL and 1.52 to 1.99 $mSvy^{-1}$, 30.99 to 37.84 Bqm^{-3}, 6.94 to 37.50 Bqm^{-3}, 0.11 to 0.86 mWL, 0.04 to 0.16 mWL and 0.89 to 1.56 $mSvy^{-1}$, 40.35 to 46.78 Bqm^{-3}, 9.72 to 26.39 Bqm^{-3}, 0.15 to 1.27 mWL, 0.05 to 0.27 mWL and 1.17 to 1.60 $mSvy^{-1}$ for granite flooring, concrete flooring, red oxide flooring, mosaic flooring and stone flooring respectively. Whereas the arithmetic mean concentrations of ^{222}Rn, ^{220}Rn, their progeny and dose rates for granite flooring, concrete, red oxide, mosaic flooring and stone flooring were 93.64, 18.85 Bqm^{-3}, 0.53, 0.06 mWL and 2.66 $mSvy^{-1}$, 80.32, 26.14 Bqm^{-3}, 0.28, 0.057 mWL and 2.44 $mSvy^{-1}$, 54.37, 26.12 Bqm^{-3}, 0.22, 0.064 mWL and 1.79 $mSvy^{-1}$, 33.98, 23.72 Bqm^{-3}, 0.26, 0.07 mWL and 1.24 $mSvy^{-1}$, 42.93, 17.56 Bqm^{-3}, 0.60, 0.14 mWL and 1.36 $mSvy^{-1}$ respectively.

Variation of indoor ^{222}Rn, ^{220}Rn, their progeny levels along with the dose rates are measured for dwellings of different floorings at Sheshadripuram, wide variations in the concentrations of ^{222}Rn, ^{220}Rn, their progeny and dose rates were observed and they were found to vary from 67.25 to 100.00 Bqm^{-3}, 17.36 to 72.92 Bqm^{-3}, 0.24 to 0.35 mWL, 0.03 to 0.15 mWL and 1.97 to 3.71 $mSvy^{-1}$, 45.03 to 52.63 Bqm^{-3}, 17.36 to 38.89 Bqm^{-3}, 0.16 to 0.35 mWL, 0.03 to 0.09 mWL and 1.41 to 1.96 $mSvy^{-1}$, 30.41 to 39.18 Bqm^{-3}, 8.33 to 40.97 Bqm^{-3}, 0.10 to 1.60 mWL, 0.03 to 0.86 mWL and 0.90 to 1.65 $mSvy^{-1}$, 10.53 to 17.93 Bqm^{-3}, 2.78 to 15.97 Bqm^{-3}, 0.04 to 0.95 mWL, 0.02 to 0.75 mWL and 0.31 to 0.71 $mSvy^{-1}$, 23.13 to 28.65 Bqm^{-3}, 7.64 to 28.47 Bqm^{-3}, 0.08 to 0.94 mWL, 0.02 to 0.24 mWL and 0.70 to 1.18 $mSvy^{-1}$ for granite flooring, concrete flooring, red oxide flooring, mosaic flooring and stone flooring respectively. Whereas the arithmetic mean concentrations of ^{222}Rn, ^{220}Rn, their progeny and dose rates for granite flooring, concrete, red oxide, mosaic flooring and stone flooring were 80.22, 40.17 Bqm^{-3}, 0.28, 0.08 mWL and 2.67 $mSvy^{-1}$, 49.13, 27.04 Bqm^{-3}, 0.21, 0.07 mWL and 1.67 $mSvy^{-1}$, 35.00, 22.32 Bqm^{-3}, 0.37, 0.17 mWL and 1.24 $mSvy^{-1}$, 14.38, 10.62 Bqm^{-3}, 0.27, 0.15 mWL and 0.53 $mSvy^{-1}$, 24.96, 16.45 Bqm^{-3}, 0.22, 0.07 mWL and 0.89 $mSvy^{-1}$ respectively.

Variation of indoor ^{222}Rn, ^{220}Rn, their progeny levels along with the dose rates are measured for dwellings of different floorings at Malleshwaram, wide variations in the concentrations of ^{222}Rn, ^{220}Rn, their progeny and dose rates were observed and they were found to vary from 81.87 to 92.9 Bqm^{-3}, 29.86 to 36.81 Bqm^{-3}, 0.29 to 0.33 mWL, 0.06 to 0.08 mWL and 2.54 to 2.94 $mSvy^{-}$

[1], 28.07 to 46.20 Bqm^{-3}, 13.74 to 34.03 Bqm^{-3}, 0.10 to 1.91 mWL, 0.04 to 0.71 mWL and 0.93 to 1.72 $mSvy^{-1}$, 19.30 to 23.39 Bqm^{-3}, 7.64 to 25.00 Bqm^{-3}, 0.06 to 0.69 mWL, 0.02 to 0.19 mWL and 0.61 to 0.99 $mSvy^{-1}$, 7.60 to 12.28 Bqm^{-3}, 2.08 to 15.28 Bqm^{-3}, 0.03 to 1.61 mWL, 0.01 to 2.45 mWL and 0.22 to 0.55 $mSvy^{-1}$, 15.20 to 17.54 Bqm^{-3}, 4.17 to 22.66 Bqm^{-3}, 0.06 to 1.60, 0.01mWL to 1.20 mWL and 0.45 to 0.81 $mSvy^{-1}$ for granite flooring, concrete flooring, red oxide flooring, mosaic flooring and stone flooring respectively. Whereas the arithmetic mean concentrations of ^{222}Rn, ^{220}Rn, their progeny and dose rates for granite flooring, concrete, red oxide, mosaic flooring and stone flooring were 87.42, 33.50 Bqm^{-3}, 0.31, 0.07 mWL and 2.74 $mSvy^{-1}$, 35.94, 25.64 Bqm^{-3}, 0.41, 0.20 mWL and 1.32 $mSvy^{-1}$, 21.76, 13.73 Bqm^{-3}, 0.23, 0.08 mWL and 0.77 $mSvy^{-1}$, 10.85, 8.74 Bqm^{-3}, 0.56, 0.55 mWL and 0.41 $mSvy^{-1}$, 16.44, 11.06 Bqm^{-3}, 0.42, 0.27 mWL and 0.59 $mSvy^{-1}$ respectively.

Variation of indoor ^{222}Rn, ^{220}Rn, their progeny levels along with the dose rates are measured for dwellings of different floorings at Jayanagar, wide variations in the concentrations of ^{222}Rn, ^{220}Rn, their progeny and dose rates were observed and they were found to vary from 53.22 to 80.56 Bqm^{-3}, 31.25 to 55.56 Bqm^{-3}, 0.19 to 2.45 mWL, 0.09 to 2.45 mWL and 1.85 to 2.93 $mSvy^{-1}$, 33.92 to 42.69 Bqm^{-3}, 12.50 to 33.33 Bqm^{-3}, 0.12 to 2.18 mWL, 0.04 to 0.82 mWL and 1.05 to 1.62 $mSvy^{-1}$, 25.15 to 29.82 Bqm^{-3}, 6.25 to 31.94 Bqm^{-3}, 0.09 to 1.08, mWL 0.03 to 0.43 mWL and 0.73 to 1.27 $mSvy^{-1}$, 12.87 to 18.13 Bqm^{-3}, 5.56 to 29.17 Bqm^{-3}, 0.04 to 1.98 mWL, 0.02 to 1.76 mWL and 0.41 to 0.93 $mSvy^{-1}$, 20.47 to 23.39 Bqm^{-3}, 12.50 to 29.89 Bqm^{-3}, 0.07 to 1.24 mWL, 0.03 to 0.93 mWL and 0.72 to 1.07 $mSvy^{-1}$ for granite flooring, concrete flooring, red oxide flooring, mosaic flooring and stone flooring respectively. Whereas the arithmetic mean concentrations of ^{222}Rn, ^{220}Rn, their progeny and dose rates for granite flooring, concrete, red oxide, mosaic flooring and stone flooring were 72.53, 46.53 Bqm^{-3}, 1.34, 0.87 mWL and 2.58, 37.35, 21.18 Bqm^{-3}, 0.54, 0.19 mWL and 1.28 $mSvy^{-1}$, 27.41, 17.01 Bqm^{-3}, 0.43, 0.18 mWL and 0.96 $mSvy^{-1}$, 15.44, 14.87 Bqm^{-3}, 0.31, 0.24 mWL and 0.63 $mSvy^{-1}$, 22.30, 19.55 Bqm^{-3}, 0.24, 0.16 mWL and 0.88 $mSvy^{-1}$ respectively.

Variation of indoor ^{222}Rn, ^{220}Rn, their progeny levels along with the dose rates are measured for dwellings of different floorings at Banashankari, wide variations in the concentrations of ^{222}Rn, ^{220}Rn, their progeny and dose rates were observed and they were found to vary from 58.48 to 89.47 Bqm^{-3}, 15.28 to 61.17 Bqm^{-3}, 0.21 to 4.46 mWL, 0.12 to 1.02 mWL and 1.72 to 3.25 $mSvy^{-1}$, 35.09 to 45.03 Bqm^{-3}, 11.18 to 60.42 Bqm^{-3}, 0.12 to 2.53 mWL, 0.02 to 1.66 mWL and 1.06 to 2.12 $mSvy^{-1}$, 21.40 to 27.49 Bqm^{-3}, 1.37 to 62.15 Bqm^{-3},

0.08 to 3.92 mWL, 0.02 to 3.93 mWL and 0.56 to 1.69 $mSvy^{-1}$, 6.43 to 12.87 Bqm^{-3}, 2.78 to 25.00 Bqm^{-3}, 0.03 to 2.23 mWL, 0.01 to 0.93 mWL and 0.20 to 0.73 $mSvy^{-1}$, 15.79 to 19.30 Bqm^{-3}, 6.18 to 40.97 Bqm^{-3}, 0.05 to 1.55 mWL, 0.01 to 2.23 mWL and 0.49 to 1.15 $mSvy^{-1}$ for granite flooring, concrete flooring, red oxide flooring, mosaic flooring and stone flooring respectively. Whereas the arithmetic mean concentrations of ^{222}Rn, ^{220}Rn, their progeny and dose rates for granite flooring, concrete, red oxide, mosaic flooring and stone flooring were 74.07, 44.67 Bqm^{-3}, 1.66, 0.42 mWL and 2.59 $mSvy^{-1}$, 38.63, 25.51 Bqm^{-3}, 0.52, 0.27 mWL and 1.39 $mSvy^{-1}$, 23.98, 22.61 Bqm^{-3}, 0.59, 0.49 mWL and 0.97 $mSvy^{-1}$, 10.55, 10.94 Bqm^{-3}, 0.29, 1.34 mWL and 0.44 $mSvy^{-1}$, 17.73, 14.57 Bqm^{-3}, 0.29, 0.27 mWL and 0.68 $mSvy^{-1}$ respectively.

Variation of indoor ^{222}Rn, ^{220}Rn, their progeny levels along with the dose rates are measured for dwellings of different floorings at Padhmanabhanagar, wide variations in the concentrations of ^{222}Rn, ^{220}Rn, their progeny and dose rates were observed and they were found to vary from 68.65 to 76.02 Bqm^{-3}, 52.99 to 70.14 Bqm^{-3}, 0.26 to 0.38 mWL, 0.13 to 0.18 mWL and 2.59 to 3.06 $mSvy^{-1}$, 41.52 to 51.49 Bqm^{-3}, 25.82 to 69.44 Bqm^{-3}, 0.14 to 1.22 mWL, 0.05 to 0.50 mWL and 1.46 to 2.43 $mSvy^{-1}$, 27.49 to 35.09 Bqm^{-3}, 6.25 to 56.25 Bqm^{-3}, 0.10 to 1.69 mWL, 0.03 to 1.91 mWL and 0.79 to 1.80 $mSvy^{-1}$, 11.70 to 16.37 Bqm^{-3}, 3.47 to 22.92 Bqm^{-3}, 0.04 to 2.02 mWL, 0.04 to 1.00 mWL and 0.35 to 0.78 $mSvy^{-1}$, 19.30 to 23.39 Bqm^{-3}, 6.94 to 34.72 Bqm^{-3}, 0.07 to 3.68 mWL, 0.02 to 9.94 mWL and 0.59 to 1.15 $mSvy^{-1}$ for granite flooring, concrete flooring, red oxide flooring, mosaic flooring and stone flooring respectively. Whereas the arithmetic mean concentrations of ^{222}Rn, ^{220}Rn, their progeny and dose rates for granite flooring, concrete, red oxide, mosaic flooring and stone flooring were 23.86, 18.11 Bqm^{-3}, 0.46, 0.57 mWL and 0.89 $mSvy^{-1}$, 46.75, 48.90 Bqm^{-3}, 0.34, 0.18 mWL and 1.97 $mSvy^{-1}$, 30.19, 26.00 Bqm^{-3}, 1.35, 3.16 mWL and 1.18 $mSvy^{-1}$, 14.03, 14.04 Bqm^{-3}, 0.52, 0.35 mWL and 0.58 $mSvy^{-1}$, 21.37, 17.80 Bqm^{-3}, 1.33, 2.37 mWL and 0.82 $mSvy^{-1}$ respectively.

Figure 4 depicts the mean concentrations of ^{222}Rn and ^{220}Rn levels in various types of floorings, as well as differences in dosage rates in various floorings. Granite floorings had higher dosage levels than mosaic floorings, which had lower dose levels. Granite flooring residences had higher ^{222}Rn and ^{220}Rn concentrations, while mosaic flooring had lower amounts. Granite is high in radium, which could explain why granite flooring houses have higher radon levels. The materials utilised in building construction are sufficiently permeable to allow radon to infiltrate the indoor environment [9]. Granite samples have a greater rate of radon exhalation than mosaic samples. There is

a positive correlation between radium content of granite with radon exhalation and its concentration [10].

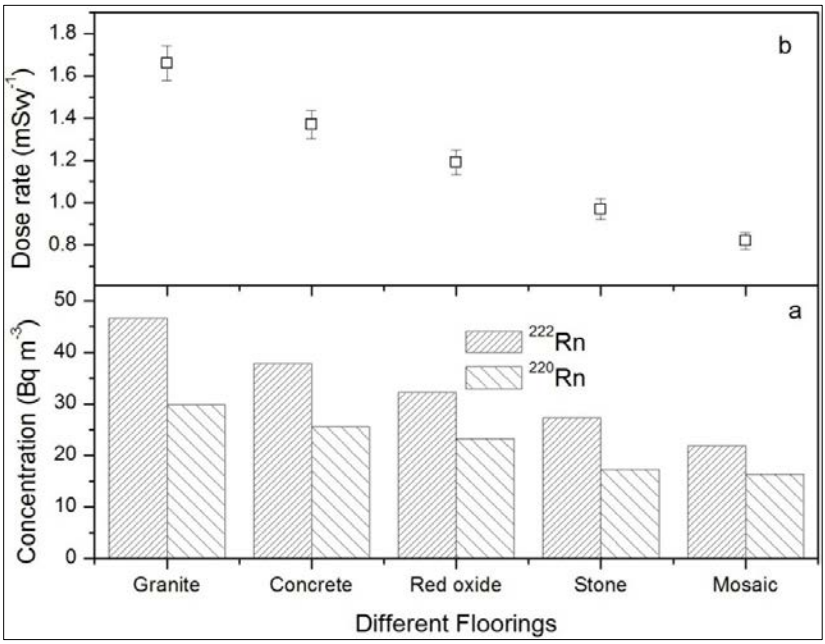

Fig 4: Floor wise ^{222}Rn, ^{220}Rn and dose rates

Figures 5 and 6 illustrate the correlations between ^{222}Rn, ^{220}Rn, and their progeny levels, as well as their frequency distributions. There was a positive association of 0.98 between average ^{222}Rn and progeny concentrations and 0.81 between ^{220}Rn and progeny concentrations.

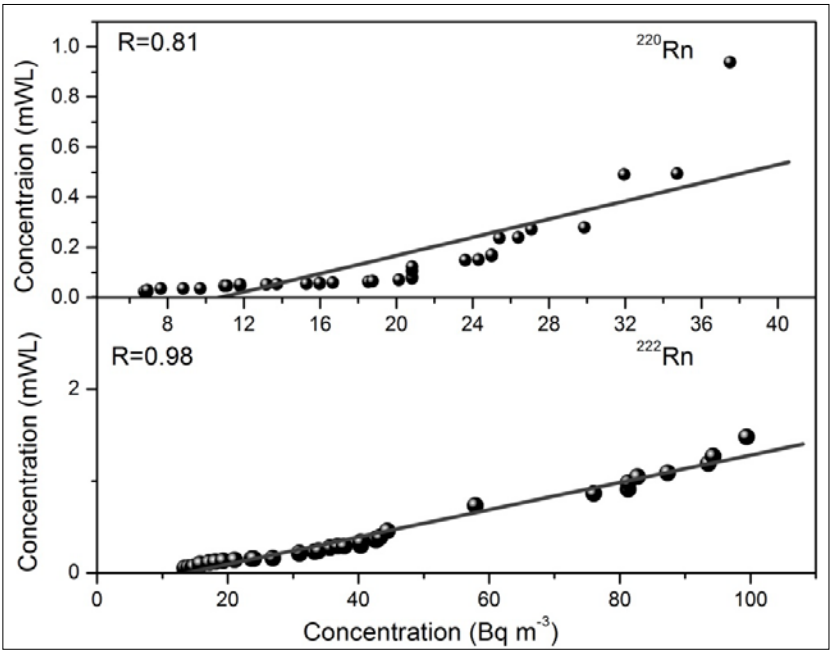

Fig 5: Correlation between radon and progenies

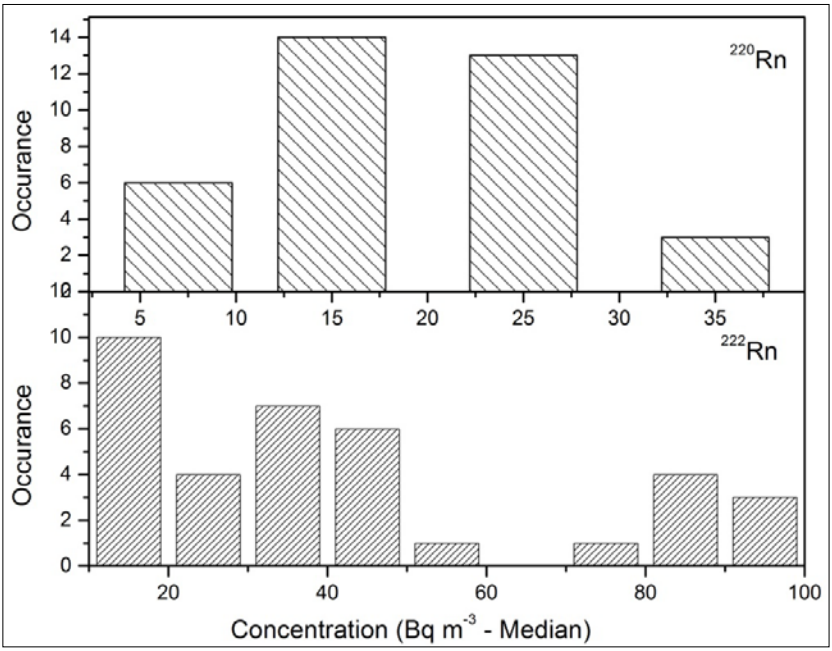

Fig 6: Frequency distribution of ^{222}Rn and ^{220}Rn

The lesser correlation could be owing to the fact that several physical and meteorological factors influence radon progeny fluctuation both indoors and outside. The difference in indoor and outdoor pressure, wind speed, wind direction, and aerosol content in the air are all important considerations (Sahota *et al*., 2005).

Conclusion

The concentration of ^{222}Rn, ^{220}Rn and ambient gamma dose were studied for dwellings with different flooring materials in different locations of Bengaluru metropolitan area. It is found that Granite floorings had higher dosage levels than mosaic floorings. This may be due to Granite has high concentration of radium and hence higher radon exhalation rates as compared to that of mosaic samples. And also the materials utilised in building construction are sufficiently permeable to allow radon to infiltrate the indoor environment. Interestingly there exists a positive association of 0.98 between average ^{222}Rn and progeny concentrations and 0.81 between ^{220}Rn and progeny concentrations for the indoor environment.

Acknowledgments

This work is carried out under UGC, New Delhi sponsored major research project in the form of research grants during 2007 to 2014 and is highly acknowledged by the author.

References

1. United Nations Scientific Committee on the Effects of Atomic Radiation, Sources, Effects and Risks of Ionizing Radiation, Report to the General Assembly, (United Nations, New York), UNSCEAR., 2000.
2. Nazaroff W. ^{222}Rn transport from soil to air., Reviews in Geophysics, 1992;302:137-160.
3. United Nations Scientific Committee on the Effect of Atomic Radiation. Sources and Biological Effects, Report to the General Assembly, (United Nations, New York), UNSCEAR, 1992.
4. Hotzal H, Winkler R. Activity concentrations of ^{226}Ra, ^{232}Th, ^{210}Pb, ^{40}K, and ^{7}Be and their temporal variations in surface air., Journal of Environmental Radioactivity. 1987;5:445-458.
5. United Nations Scientific Committee on the Effects of Atomic Radiations. Sources and Effects of Ionizing Radiation, (United Nations : New York), 77, UNSCEAR, 1993.
6. Sathish LA, Nagaraja K, Ramanna HC, Nagesh V, Sundareshan S.

Concentration of radon, thoron and their progeny levels in different types of floorings, walls, rooms and building materials., Iranian Journal of Radiation Research. 2009;7(1):1-9.

7. Srivastava GK. A study of the potential internal radiation hazards and their control in Uranium mining and milling. Ph.D. Thesis, University of Bombay, 1994.
8. Kamsali Nagaraja, Prasad BSN, Datta J. Atmospheric electrical conductivity measurements and modeling for application to air pollution studies, Advances in Space Research. 2009;44(9):1067-1078.
9. Gaso MI, Segovia N, Pulinets S, Leyva A, Ponciano G, Pena P. Indoor radon and annual effective doses at a high-altitude region in central Mexico., Journal of Applied Science. 2005;5:1356-1362.s
10. Al Jarallah M. ^{222}Rn exhalation from granites used in Saudi Arabia., Journal of Environmental Radioactivity. 2001;53:91-98.
11. Sahota HS, Randhawa KS, Singh M, Singh K. Temperature variation of indoor and outdoor radon progeny., Atmospheric Environment. 2005;39(16):2991-2994.

Chapter - 5
Characterization and Preparation Methods of Semiconductor Photocatalysts

Author

Dr. Sagar Ranjan Kande

HOD, Assistant Professor in Chemistry, Department of Chemistry, New Arts, Commerce and Science College, Shevgaon, Ahmednagar, Maharashtra, India

Chapter - 5

Characterization and Preparation Methods of Semiconductor Photocatalysts

Dr. Sagar Ranjan Kande

1.1 Introduction

The co-doped semiconductor photocatalysts like SnO_2, ZnO-SnO_2, CdS and ZnO supported on active carbon were synthesized using conventional as well as new preparation methods. The precipitation, co-precipitation, sol-gel and hydrothermal methods were used for the synthesis. It is always be a challenge for researchers to use the specific method which give high yield, low toxic byproducts and low cost [1-2]. It is also known that the morphology, size and properties of prepared photocatalysts depend on the method used [3-4]. The search of different co-doped semiconductor materials supported on active carbon has encompassed us to use various chemicals, solvents and instruments. The synthesized materials further analyzed by different chemical and physical methods.

1.2 Physico-chemical characterization methods

1.2.1 X-ray powder diffraction (XRD)

X-ray powder diffraction is a rapid, non-destructive analytical technique used to investigate the structure of a crystal. Each crystal structure has its characteristic XRD pattern with different intensities and position of diffraction peaks [5]. This gives very important information about its crystalline phases and structure. The relative concentration of each phase can also be studied by XRD pattern [6]. When X-ray radiation with wavelength λ constructively interfaces the crystal, XRD pattern is formulated after satisfying bragg's condition:

$$n\lambda = 2d\sin\theta;\ n = 1,\ 2,\ 3,..... \quad (2.1)$$

Where d is the d-spacing (distance between adjacent planes), θ is the angle of incident and n denotes the layer of plane. In a typical experimental procedure the powder sample is pressed into a sample holder to make a flat surface. When X-ray radiation hits on the atoms in the sample the electrons

present in the atom starts to oscillate with similar frequency of X-ray radiation. This process generates constructive or destructive interfaces. The planes which having high electron density shows strong reflection and intensity [7]. On the other hand the planes with less electron density show less reflection and low intensity. Accordingly, the XRD diffraction technique is useful for identification and characterization of polycrystalline phases of the sample

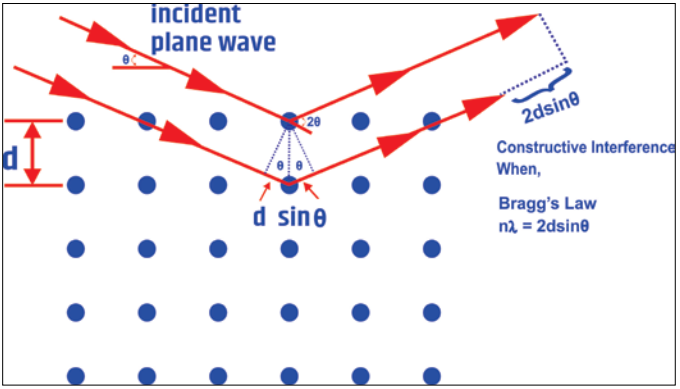

Fig 1: Bragg's law

Average crystalline size of nanocrystals can be calculated from wavelength, peak position and its full width at half maxima (FWHM) using scherrer's equation:

$$D = \frac{0.9\lambda}{\beta \cos\theta}$$

Where D is the crystalline size, λ is the wavelength of the X-ray radiations (1.542 A°), θ is the scattering angle of the diffraction peak and β is the FWHM. X-ray powder diffraction pattern of prepared sampled were carried out on Brucker D8 Advanced diffractometer using Cu Kα radiation source at 40 kV, 30 mA over 2θ range of 20-80º.

1.2.2 Surface area (BET) measurement

Measurement of surface area is very important in the study of powder sample. The Brunauer, Emmett and Teller developed an important method to study the textural characterizations like surface area, pore volume and pore size using N_2 gas as an adsorbent gas [8-9]. In this study these textural properties were studied by N_2 adsorption isotherm measurement using Micrometrics ASAP 2020 Brunaur Emmett Teller surface area analyzer. This study is known as an extension to the multilayer adsorption of the

Langmuir model. In this process the chemisorptions is restricted to the monolayer adsorption at the surface. The volume of the adsorbed gas (generally N_2) on the surface of particles is recorded at boiling temperature of nitrogen (-196ºC). The general BET equation is given as:

$$\frac{1}{V\left[\left(\frac{P_0}{P}\right)-1\right]}=\frac{1}{V_m C}+\frac{C-1}{V_m C}\left(\frac{P}{P_0}\right) \tag{2.2}$$

Where V is the adsorbed gas volume at relative pressure P, V_m is the volume of gas adsorbed from monolayer of surface coverage, C is the BET constant and P_0 is saturation pressure. To calculate V_m and C, the BET equation is plotted as an adsorption isotherm between 0.05-0.35 relative pressure. The V_m is found from gradient and then surface area can be obtained using the molecular cross-sectional area,

$$S_{BET}=V_M \cdot N_A \cdot A_M \times 10^{-20} \tag{2.3}$$

Where, V_m - moles of nitrogen molecules adsorbed,

N_A – Avogadro number (6.023×10^{23} molecules/mol)

A_M – cross-sectional area of adsorbate gas (N_2 molecules, 16.2Aº)

1.2.3 Scanning electron microscopy (SEM)

The Scanning electron microscopy is one of the important type of electron microscope that produce high resolution images with good depth of field of sample by rastering a high energetic electron beam on a fine scale and detecting secondary and back scattered electron signals under vacuum [10-11].

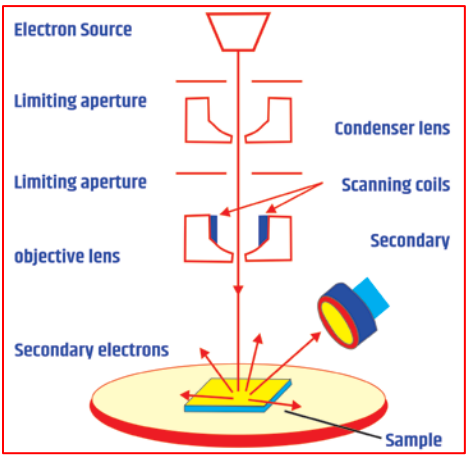

Fig 2: Schematic diagram of scanning electron microscope (SEM)

Fig. 2. shows that the highly energetic electron beam is travel through scan coils and objective lens. Further this beam is get deflect vertically as well as horizontally. Commonly, during the SEM analysis the atoms are excited by the high energy electron beam which gives emission of secondary electrons. These secondary electrons are further detected by detector. After scanning the sample and analyzing the secondary or back scattered electrons, an image is obtained which shows the topology of the surface of sample. In addition to this the elemental analysis of sample is another application of this microscopy known as Energy Dispersive X-ray microanalysis (EDX). The irradiation of electrons of the sample results in the vacancy of electron which is occupied by other electron from higher energy orbital [12]. To balance the difference in energy levels between the two electrons the X-ray radiations emitted. The analysis of X-ray radiations emitted versus the energy of electrons gives EDX spectra. SEM analysis gives images which have resolution higher than 1 nm. In the present study SEM images were obtained from FEI Nova NanoSEM 450.

1.2.4 UV-visible diffuse reflectance spectroscopy (UV-vis DRS)

UV-vis DRS spectroscopy provides us information about structure of the molecules [13]. The absorption of UV and visible light by many molecules causes electronic excitations which move electrons from ground state to excited state [14]. The absorbed light is reflected in all directions. The small fraction of this light is scattered within the sample and then come to its surface is known as diffuse reflection. After amplifying the signal to noise ratio of the collected reflected radiations give UV-vis DRS spectra. The absorption of light energy by molecules is governed and formulated by Beer-Lamberts law as:

$$A = \varepsilon \cdot c \cdot l$$

Where A, ε, C and l are absorbance, absorptivity, concentration and length of the cell respectively. Moreover; the absorbance is also depend on size of molecules, and type of sample. If the size of molecule is much higher than wavelength of absorbed light then scattering and reflection is observed. Therefore for powder samples the UV-vis DRS analysis is based on Kubelka-Monk equation:

$$F(R) = \frac{(1-R)^2}{2R}$$

Where F(R) is equivalent to absorption coefficient and R is diffuse

reflectance at front face. The bandgap energy was calculated by using following equation:

$$\alpha\left(h\nu\right) = A\left(h\nu - E_g\right)^n \tag{2.4}$$

Where α, h, ν, A and E_g are the absorption coefficient, planck's constant, frequency of absorbed light and bandgap energy. n is obtained from type of semiconductor used.

1.2.5 Transmission electron microscopy (TEM)

Transmission electron microscopy is an important analytical technique for directly imaging nanomaterials to obtain quantitative measures of particles, grain size, size distribution and morphology [15]. In this technique a high energy electron beam is transmitted through a very thin sample. After interaction of electron and atoms of molecule show scattering of electrons. Further, these scattered electrons projected onto a fluorescent screen and gives crystal structures, grain boundaries and dislocation of atoms. TEM spectroscopy has ability to give high resolution images compared to other microscopes [16]. The shape, size, quality of sample, density of quantum walls and dots can be examined through high resolution images. In addition to this the finest details of internal structure of molecules can also be studied by transmission electron microscopy. The electron density variations as well as analog images may be obtained using CCD camera. In this study, TEM and HRTEM images were obtained from FEI Tecnai F30 operated at 300kV.

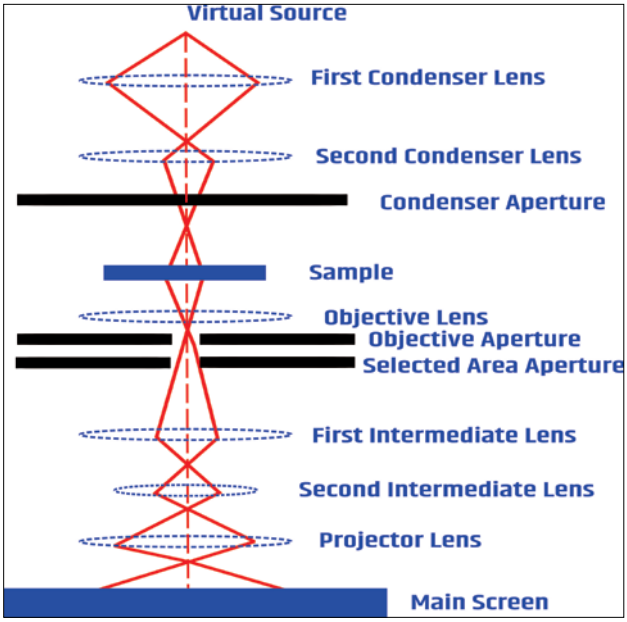

Fig 3: Diagram of transmission electron microscope (TEM)

1.2.6 Fourier transform infrared spectroscopy (FTIR)

FTIR spectrum of sample provides good deal of information about structure of synthesized metal oxides [17]. In this spectroscopy, when sample is exposed to IR radiations, the molecule absorbs energy of IR radiation and gets excited to higher vibration energy level. The type of IR wavelengths absorbed by the molecule depends on the type of atoms and chemical bonds in the molecule. The IR spectrum consists of number of peaks; each peak is due to a particular vibration excitation of the molecule [18]. The IR spectrums in the present study were recorded using avatar-330 spectrophotometer at room temperature in the range of 400-4000 cm^{-1}.

1.2.7 Photoluminescence (PL) spectroscopy

Photoluminescence is a non-destructive technique used to probe the efficiency of charge carriers trapping and e/h pair recombination during photocatalysis of the sample [19]. Photoluminescence spectroscopy is based on the emission of the light by sample after the absorption of electromagnetic radiations. Absorption of these electromagnetic radiations results photoexcitation of electrons. The excited electrons return to their ground state, the excess energy is released out in the form of emission of light. It is well known that more the PL intensity, the lower e/h pair

recombination and lower charge carriers separation efficiency. Photoluminescence (PL) emission spectra of prepared photocatalysts at room temperature were obtained using SCINCO FluoroMate FS-2.

1.2.8 X-ray photoelectron spectroscopy (XPS)

X-ray photoelectron spectroscopy is a quantitative spectroscopic technique with high surface sensitivity [20]. This technique is used to study the empirical formula, chemical states and elemental composition of the sample. A monochromatic beam of aluminum and magnesium X-ray is allowed to irradiate the sample. The electrons from core levels of atoms get excited and ejected. These ejected electrons from the 1-10 nm top layer having kinetic energy and it is analyzed by hemispherical electron energy analyzer.

The binding energy given in the XPS spectrum is the elemental fingerprint [21]. This gives useful information about surface elemental composition of sample. In addition to this the chemical environment around atoms, charge and ionic state information can also be obtained. The B.E. of ejected electrons is calculated by following equation:

$$E_{BE} = h\nu - E_{KE} - \phi \qquad (2.5)$$

Where, h, ν and ϕ are the plancks constant, frequency of exciting energy source and work function of spectrometer respectively. In the present study ESCA-3000, VG Microtech was used to investigate the chemical composition of the prepared photocatalysts.

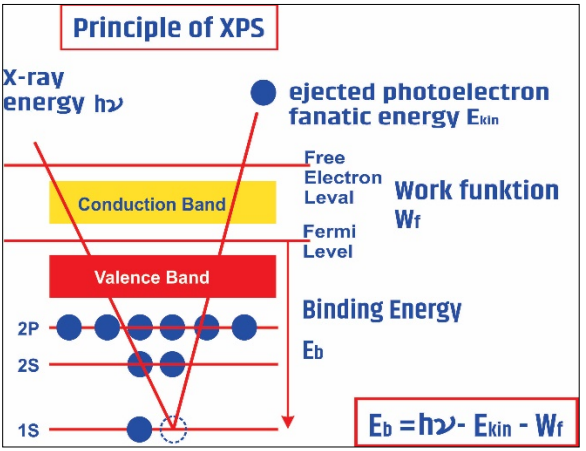

Fig 4: Schematic representation of principle of X-ray photoelectron spectrometer (XPS)

1.2.9 Raman spectroscopy

Raman spectroscopy is commonly used in chemistry to study the structural fingerprint of the molecules by which molecule can be identified [22]. The principal of Raman spectroscopy is based on the probing of inelastic scattering of the irradiated monochromatic light after its interaction with sample. The peaks observed in Raman spectra are due to vibration, rotational and low frequency modes in the system [23]. The size of the nanocrystals can also be investigated using phonon confinement effect. Those molecular vibrations of the sample which are polarizable can produce Raman shifted photons, so this method is also known as complimentary to IR spectroscopy. Raman spectroscopy is a useful technique to study the structural phases as well as binding configurations of sample. In this study, Raman spectra were recorded on Renishaw InVia Raman spectrometer at room temperature.

1.3 Methods for the synthesis of photocatalysts

1.3.1 Precipitation method

The formation of solid compound in solution during a chemical process is known as precipitation method [26]. When the reaction is carried out in liquid solution, the solid is get settled at bottom called as precipitate and the rest liquid part is known as supernatant. During the process the formed solid compound in solution is get settle at bottom due to gravitational force or centrifugation. The precipitation occurs only if generated insoluble material has higher density. It is well known that when the material is present in solution is above its solubility limit lead to precipitate. This method is very useful to synthesize the nanoparticles of various photocatalysts. Nucleation is also an important step during precipitation. The generation of solid particles at interface requires relative surface energy. The reaction shows supersaturation without this energy.

1.3.2 Hydrothermal method

Hydrothermal is one of the important technique used to synthesize the good quality nanocrystals. The size of synthesized crystal is depends on the solubility of minerals in high temperature and pressure of water [27]. This process is generally carried out in teflon lined stainless steel autoclave containing aqueous solution at high temperature and pressure. Further the temperature is increased above the boiling point of solution to get the pressure of vapor saturation. Water is acts as solvent in the recrystallization. The solid material is synthesized during this process. Size, morphology and surface properties of prepared solids can be easily controlled through monitoring the solvent, pressure and temperature during the process. The

crystalline phases which are unstable at the melting point as well as those which have high vapor pressure, can be synthesized using hydrothermal method.

1.3.3 Sol-gel method

Variety of nanosized semiconductor photocatalysts can be prepared by sol-gel method. The morphological as well as chemical properties can be easily controlled by this method [28]. Several oxides in the form of thin films, porous membrane, powders can be synthesized by sol-gel method. The sol-gel method is commonly used to synthesize semiconductor photocatalyst with high surface area which is difficult to obtain by conventional methods. In addition to this the mixing level of ingredients is retained in the synthesized compound. This method is also found successful in the production of stained glass. The composition of product can be easily controlled through cheap and low temperature sol-gel method. Even very small quantity of dopant can be uniformly introduced using this method. In the general sol-gel method colloidal suspension i.e. sol is formed from hydrolysis and polymerization process. Metal alkoxides and metal salts are used as a precursor to prepare sol.

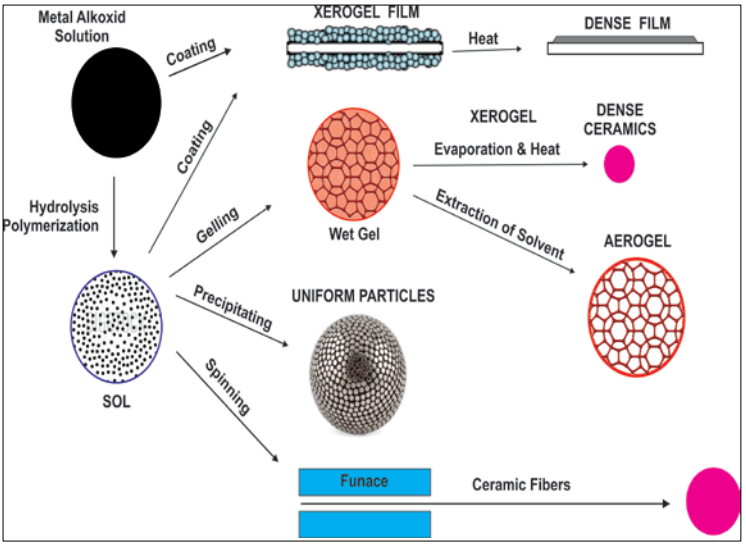

Fig 6: Schematic drawing of sol-gel method

This sol can be used to make dense films, ceramics, ceramic fibers etc [29]. After transfer of sol into mold it gives gel. Further drying and heating gives glass and ceramic materials. The obtained products from sol-gel method have various applications in thin films, coating materials, nanoscale

powders etc.

1.3.4 Co-precipitation method

The carrying down by a precipitate of material, which is soluble under the reaction conditions, is called as co-precipitation method [30].

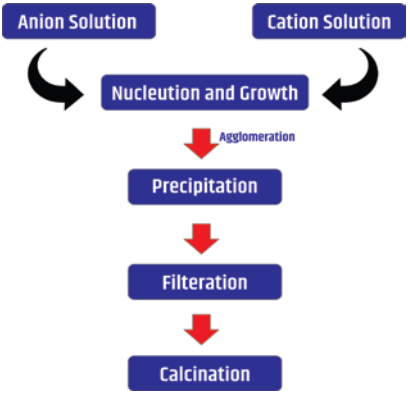

Fig 7: Schematic representation of co-precipitation method

It is well known that separation of a crystalline precipitation from the solution is difficult task as it may contain some impurities from mother liquor. The digestion of the solution is found as a solution to mitigate this problem. Generally, there are three different mechanisms of co-precipitation method i.e. inclusion, occlusion and adsorption. There are several applications of co-precipitation method apart from chemical analysis i.e. wastewater demineralization, radionuclide migration etc.

1.5 Surfactants

Surfactants are the compounds which have characteristic structure and commonly used as a dispersant in nanoparticle synthesis [31-32]. Surfactants can lower the surface tension between two liquid so it is also known as wetting agent. Surfactants consist of both hydrophilic and hydrophobic groups. Surfactants play vital role industrial processes as it can be act as dispersant, emulsifiers, wetting and foaming agent. Generally, there are four different types of surfactants- nonionic, anionic, cationic and amphoteric.

Nonionic: Polypropylene glycol, sorbitan alkyl ester etc.

Anionic: Sodium stearate, Lignosulfonate, Sodiun loryl ethyl sulphate etc.

Cationic: BAC, CPC, CTAB-(Cetyl trimethyl ammonium bromide), CTAC etc.

Amphoteric: CHAPS 3-[(3-Cholamidopropyl)dimethylammonio]-1-propane sulfonate.

References

1. Asahi R, Morikawa T, Ohwaki T, Aoki K, Taga Y, Science. 2001;293:269-275.
2. Begum NS, Ahemad HMF, Hussain OM. Bull. Mater. Sci. 2008;31:741-749.
3. Das D, Mishra HK, Parida KM, Dalai AK. Journal of Molecular Catalysis A. 2002;189:271-279.
4. Gambhire AB, Lande MK, Arbad BR, Rathod SB, Gholap RS, Patil KR. Materials Chemistry and Physics. 2011;125:807-810.
5. Tebby Z, Babot O, Toupance T, Park DH, Campet G., Delville MH, Chem. Mater. 2008;20:7260-7269.
6. Parida KM, Dash SS, Das DP. J. Colloid Interface Sci. 2006;298:787-792.
7. Wachs IE, Roberts CA. Chem. Soc. Rev. 2010;39:5002-5007.
8. Rouquerol J, Llewellyn P, Rouquerol F. Studies in Surface Science and Catalysis. 2007;160:49-54.
9. Hanaor DAH, Ghadiri M, Chrzanowski W, Gan Y. Langmuir, 2014;30:15143.
10. Hortola P. Microscopy and Microanalysis. 2015; 21:1504-1510.
11. Tahmasebi P, Sahimi M, Physical Review E. 2012;85:066709.
12. Klein T, Buhr E, Frase CG, Advances in Imaging and Electron Physics. 2012;171:297-304.
13. Soovali L, Room EI, Kutt A. Accreditation and Quality Assurance. 2006;11:246-254.
14. Ansell S, Tromp RH, Neilson GH. J. Phys.: Condens. Matter., 1995;7:1513-1520.
15. Ross B. Science. 2015;350:1490-1499.
16. Kosasih FU, Ducati C. Nano Energy. 2018;47:243-254.
17. Manor J, Feldblum ES, Arkin IT. The Journal of Physical Chemistry Letters. 2012;3:939-945.
18. Brielle ES, Arkin IT. The Journal of Physical Chemistry Letters, 2018;9:4059-4066.

19. Kaindl RA, Carnahan MA, Hagele D, Lovenich R, Chemla DS. Nature, 2003;423:734-741.
20. Ray S, Shard AG. Analytical Chemistry. 2011;83:8659-8666.
21. Gumerova NI, Rompel A. Journal of Catalysis. 2014;311:369-375.
22. Itoh Y, Hasegawa T. The Journal of Physical Chemistry A. 2012;116:5560.
23. Schlucker S. Journal of Biophotonics. 2011;4:453-461.
24. Silva CG, Wanga W, Selvam P, Dapurkar S, Faria JL. Studies in Surface Science and Catalysis. 2006;162:151-160.
25. Amrhein K, Stephan D. Photochem. Photobiol. Sci. 2011;10:338-345.
26. Xu L, Wei B, Liu W, Zhang H, Su C, Che J. Nanoscale Research Letters. 2013;8:536-542.
27. Dhal JP, Mishra BG, Hota G. RSC Adv. 2015;5:58072.
28. Tseng TK, Lin YS, Chen YJ, Chu H. Int. J. Mol. Sci. 2010;11:233-240.
29. Shukla P, Shukla JK. J. Sci.: Adv. Mater. Devi. 2018;3:452-463.
30. El-Shazly AN, Rashad MM, Abdel-Aal EA, Ibrahim IA, El-Shahat MF, Shalan AE. J. Environ. Chemi. Eng. 2016;4:317-322.
31. Metcalfe TL, Dillon PJ, Metcalfe CD. Environ. Toxicol. Chem. 2008;27:811-819.
32. Scott MJ, Jones MN. Biochim. Biophys. Acta. 2000;1508:235-240.

Chapter - 6
Preparation and Characterization of Carbon Black Reinforced Natural Rubber Composite Materials

Authors

Rekharani Maddula
Assistant Professor, Department of Physics, Gokaraju Lailavathi Womens Engineering College, Hyderabad, Telangana, India

Kesava Vamsi Krishna Vajjala
Associate Professor, Department of Physics, Malla Reddy Engineering College (A), Hyderabad, Telangana, India

Etta. Udayasri
Lecturer, Department of Commerce, Indira Priyadarshini Govt. Degree College for Women, Hyderabad, Telangana, India

Chapter - 6

Preparation and Characterization of Carbon Black Reinforced Natural Rubber Composite Materials

Rekharani Maddula, Kesava Vamsi Krishna Vajjala and Etta. Udayasri

Abstract

The properties of polymers are enhanced by addition of filler/additive. The former part of present research dwells upon discussion on carbon black (CB) powder and then its application in rubber technology. The three industrial grades of carbon black (CB) namely N405, N375 and N509 were selected to inspect the suitability and application of these grades that are of commercial interest. The particle size, surface area and structure are the three fundamental characteristics of CB powder that determine their process ability and application as filler in preparing rubber compounds. These CB powder grades were primarily characterized for their physical properties prior to mixing them in natural rubber (NR) matrix. The powders were characterized for their structure using dibutyl phthalate absorption (DBPA), particle size via laser particle size analyzer, surface area by nitrogen adsorption method, pellet hardness by means of pellet hardness tester. The CB powders were also characterized by X-ray diffraction (XRD) and Fourier transform infrared spectroscopy (FTIR). These grades were mixed with NR matrix along with other constituents via two roll mill and CB reinforced with natural rubber (CBNR) composites were synthesized.

Keywords: Carbon, rubber, composite materials

1. Introduction

Elastomers are cross-linked polymers possessing low modulus and high deformation reversibility, affirming their utility in wide range of applications [1-2]. The CB is used as a principal reinforcing filler for NR because it enhances the physical and chemical adsorption of elastomer molecules on its surface. This was due to the presence of CB specific structure and organic functional group (mainly, –OH).

The three main contributions responsible for this reinforcement are:

i) Hydrodynamic effect related to the gain in strength by dispersion of inclusion in a rubber matrix.

ii) Polymer-filler interconnection responsible for modified rubber layer.

iii) Percolating point associated with agglomerated framework [3-4].

The significant role of CB as active filler in elastomers for tyre technology has been known for more than a century [5]. This reinforcement of elastomer with CB increases their mechanical properties such as tensile strength, resilience, elastic modulus and hysteresis that find application in anti-vibrating operations of industries. Thus, it is agreeably recognized that CB filled rubber composites having multiphase system, dependent on the mobility of rubber molecules, impacts the reinforcement of the composites. The viscosity of NR is reduced by mixing it with peptizers and subjecting it to a shearing process. The service span and mechanical efficiency can be notably improved by mixing fillers in elastomer matrix.

Park *et al*. investigated the interrelation of mechanical properties with the surface energy of CB and had established that the specific surface area increases non-polar characteristics. This further increases mechanical properties and improves vulcanization reactions of the composites. Moreover, previous researchers had examined the key function of networking fillers on the properties of elastomer composites. They had elucidated that the filler-filler interaction play an integral role in influencing reinforcement mechanism in composites. The chemical and physical synergy between polymer matrix and CB affect the mechanical and curing characteristics had also been previously examined. There had been continuous interest towards studies on dependence of size, structure and surface activity of CB on the properties of CB composites but few investigations have been reported on studies of different grades of CB [6].

The effects of three different grades of CB on the curing and mechanical properties of the CBNR composites have been investigated. Additionally, the variation in properties of CBNR composites due to particle size and surface chemistry were of importance, as done previously. The three industrial grades (N375, N405 and N509) were chosen to examine the differences that are of commercial interest between N405 with that of N375 and N509. These grades of CB powder were initially characterized for their physical characteristics before mixing it with NR. The standard procedures were followed for synthesis and vulcanization of different rubber composites. And

the ASTM standards were adhered to, for testing characteristics, in order to gain insight into the influence of different grades of CB on CBNR composites [7-8].

2. Studies on CBNR Composites

The NR, is an elastic polymeric material with monomer unit Isoprene (2 methyl butadiene), acquired from the latex of trees sap (particularly trees belonging to the genera of Ficus and Hevea) that are vulcanized and finished for different useful applications. The prime parameters related to vulcanization process can be determined using rheometer, with 1.7 Hz oscillation frequency and 145 °C die temperature, for assessing the rate of cross-linking and curing due to the CB-rubber interactions. The vulcanization curves of CBNR composites, associated with various grades of CB are displayed in Figure 1 and 2. The cure characteristics: M_L (minimum torque), M_H (maximum torque), T_{c90} (optimum cure time), T_{s2} (scorch time) of CBNR composites with three different grades of CB such as N375, N405 and N509 were determined from the curve as shown in Table.1. The vulcanization rate, dependent on the difference between the initial scorch time (t_{s2}) and optimum cure time (t_{c90}), is ascertained by CRI, given by Equation (1) and is based on ASTM standard D2084 [9-10].

$$CRI = \frac{100}{T_{c90} - T_{s2}} \tag{1}$$

The CRI values calculated for CBNR composites using N375, N405 and N509 were 0.090, 0.105 and 0.093 s^{-1}, respectively. Thus, it was observed that the fastest cure rate and optimum cure time resulted in highest CRI for N405 composite. The decreased cross-linking speed due to the existence of quinolic group caused lowest CRI for N375 composite [11].

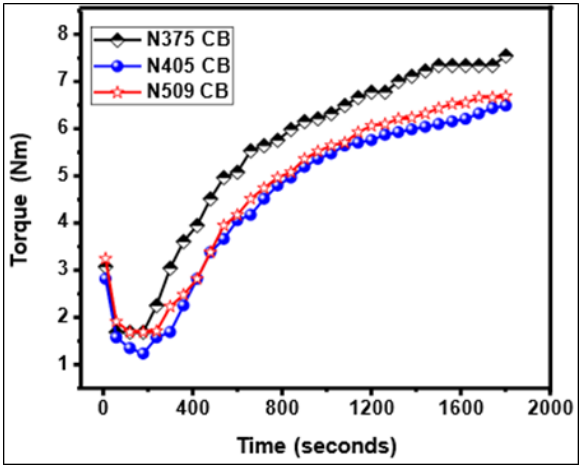

Fig 1: Vulcanization curves between torque versus time of CBNR composites at 145 °C, associated with various grades of CB (N375, N405 and N509)

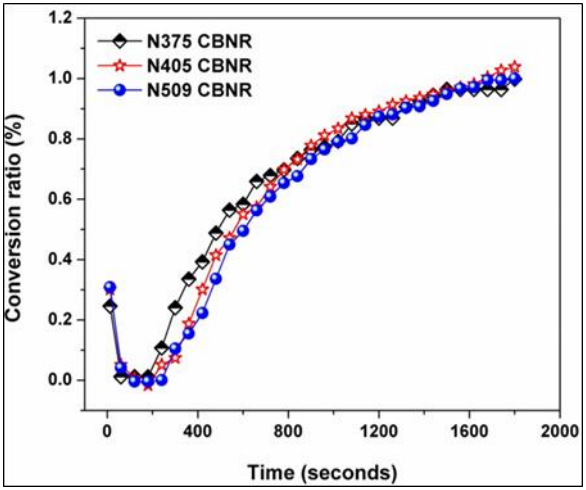

Fig 2: Conversion ratio of CBNR composites for N375, N405 and N509 grades of CB as a function of cure time

Table 1: Rheometric data comprising of maximum torque M_H (Nm), minimum torque M_L (Nm), $M_H - M_L$ (Nm), scorch time T_{s2} (sec), optimum cure time T_{c90} (sec), cure rate index (CRI) for CBNR composites with different grades of CB

CBNR Composites of different grades	M_H (Nm)	M_L (Nm)	M_H-M_L [a] (Nm)	*Ts2* [b] (sec)	*Tc90* [c] (sec)	CRI [d] (sec^{-1})
N375	7.56	1.62	5.93	194.4	1309.2	0.090
N405	6.30	1.32	4.98	256.8	1212.0	0.105
N509	6.69	1.71	4.98	260.4	1332.6	0.093

a) Difference between maximum and minimum torque.

b) Scorch time, time at which the vulcanization begins (derived from the measurement done on Monsanto Rheometer).

c) Optimum cure time, time needed for curing of rubber samples (derived from the measurement done on Monsanto Rheometer).

d) Cure rate index determined from rheological testing using Equation (1).

The difference ΔM (= M_H-M_L), the characteristic of cured rubber, provides the information on degree of chemical cross-linking which occurs during the process of vulcanization. The property that varies with the surface area of different CB is modulus at 300% elongation along with M_L. The surface area of CB plays a significant role in the physical cross-linking of CBNR composites. The increase in the number of rubber chains entangled with CB aggregate enhances with the CB surface area. This entanglement of polymer chains with CB further enhances the torque, and thus CB serves as physical cross link in CBNR composite. Therefore, it can be noticed that N509 grade CB having highest NSA showed largest value of M_L out of the three different grades of CB. This was due to the decrease in the number of mobilized rubber chains on CB surface [12-13].

The flat rubber composite sheets were made, according to the ASTM standard D2084, by using hydraulic press that was heated electrically to vulcanize compounds at 145 °C and for cure times, T_{c90}. The conversion rate of vulcanization χ_T for a given time had been evaluated from the RHEO curves using Equation (2) and is depicted in Figure 2.

$$\chi_T = \frac{M_T - M_L}{M_H - M_L} \tag{2}$$

Here, M_T denotes the torque at a given time T; while M_L and M_H are the minimum and maximum torques, respectively. The Figure 2 shows the conversion ratio of composites of CBNR for various grades of CB as a function of time of cure. Thus, the conversion rate of vulcanization for CBNR composites at these specified conditions show the order as N375 > N405 > N509. Here, in order to complete 50% conversion, N375 CBNR takes 491 s, N405 CBNR takes 561 s and N509 CBNR takes 609s. This confirms that all the vulcanization characteristics vary proportionately with the increase in surface area. The rheological test, exhibited lowest CRI for N375 rubber composite having highest RSF, which is illustrated in Figure 3.

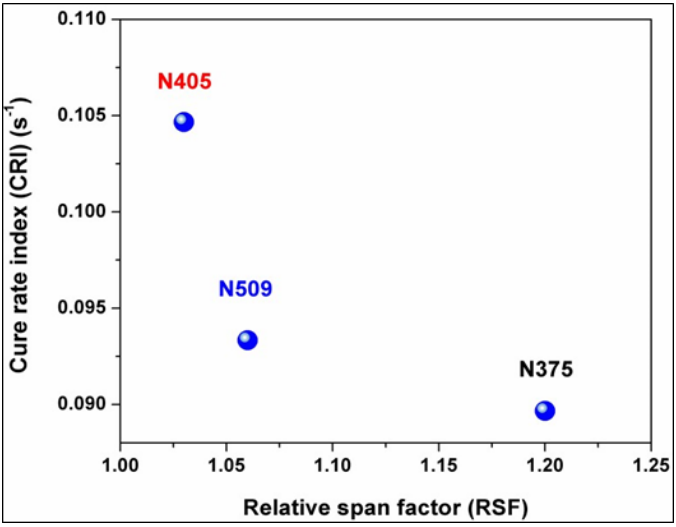

Fig 3: CRI of CBNR composites as a function of RSF of CB powders

3. Mechanical testing

The mechanical properties of CBNR composites made by furnace CB were inspected by employing universal electric tensile testing (Zwick 1435) machine. Here, dumbbell sections of 25 x 10^{-3} m width, 130 x 10^{-3} m length and 2 x 10^{-3} m thickness were cut with the help of die cutting machine. The tensile strength and elongation at break; as well as modulus at 200% and 300% elongation were determined according to ASTM method D412-06a at 5 kN load and test speed of 0.008 ms^{-1}. The stress-strain profile for different CBNR composites are shown in Figure.4, whereas tensile strengths and modulus at 300% elongation along with their respective errors are illustrated as histogram in Figure.5. Here, Table.2 depicts the different reinforcing abilities of the composites by listing mechanical properties such as tensile strength, elongation at break, modulus at 200% elongation and modulus at 300% elongation of CBNR composites. The factors that affect the modulus at 300% elongation are shape of the particles and surface activity including surface treatment. It was observed that the tensile strength of CBNR composites increase with increasing surface area of CB powder. N509 rubber composite, having largest surface area showed highest tensile strength among all grades of CB. Further, RSF was found to have correlation with elongation at break. N405 possessing lowest RSF showed maximum elongation at break. Thus, the extent of formation of weak bonds, by physical adsorption on filler surfaces to affix polymer chains, is influenced by the surface area [14-15].

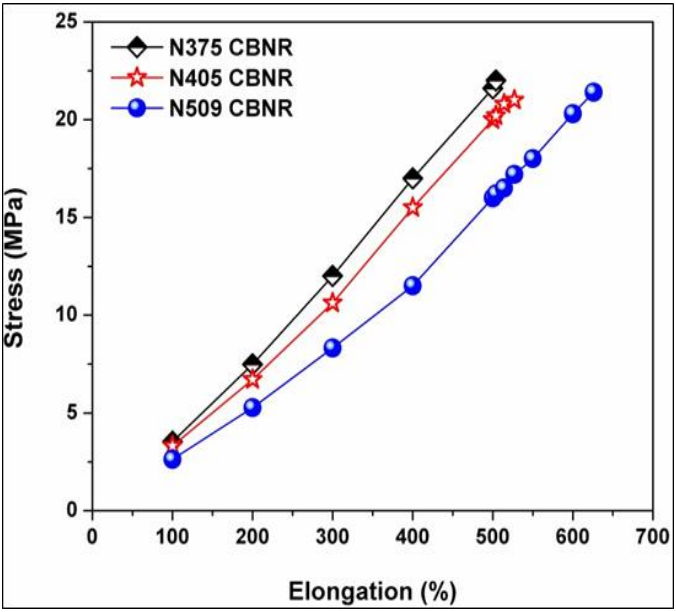

Fig 4: Stress-Strain curve of N375, N405 and N509 grades of CB obtained from tensile testing machine Zwick 1435

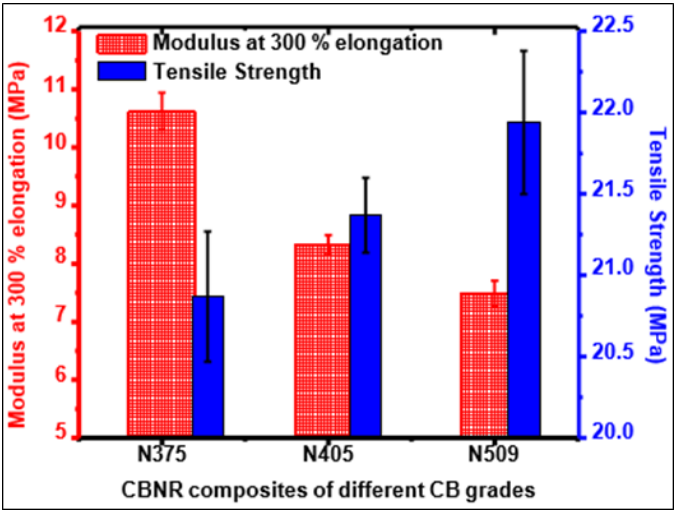

Fig 5: Histogram for modulus at 300% elongation and tensile strength of CBNR composites

Table 2: Reinforcing abilities of the composites using N375, N405 and N509 grades of CB having tensile strength (MPa), elongation at break (%), modulus at 200% elongation and modulus at 300% elongation

CBNR composites	Tensile Strength (MPa)	Elongation at break (%)	Modulus at 200% elongation (MPa)	Modulus at 300% elongation (MPa)
N375	20.87±0.40	527±14	6.71±0.25	10.62±0.32
N405	21.37±0.23	626±5	5.27±0.09	8.32±0.17
N509	21.94±0.44	504±9	3.53±0.21	7.49±0.22

4. Hardness and Resilience testing

The Durometer is a standard device that is used to assess the hardness of rubber, polymers or rubber-like materials. It measures the hardness by the penetration of an indenter into the material and is expressed as a number value. Here, Shore hardness was measured before and after curing (Figure 6 and Figure 7) of rubber samples as outlined in Table. 4. The hardness increased with the increasing surface area as N375 < N405 < N509 for cured CBNR composites, similar to Litvinov's report. The highest NSA and STSA depicted by N509 CB powder had highest hardness of its CBNR composite. This implies that surface area is a vital criterion in determining the hardness behaviour of CBNR composites [16].

Resilience usually expressed in percentage is stated as the ratio of energy given up in retrieval from deformation to the energy needed to cause the deformation. Table. 3 shows the trend of resilience observed for vulcanized CBNR composites as N375 < N405 < N509. It can be readily ascertained from the examination that the resilience of CBNR composites almost doubled after vulcanization.

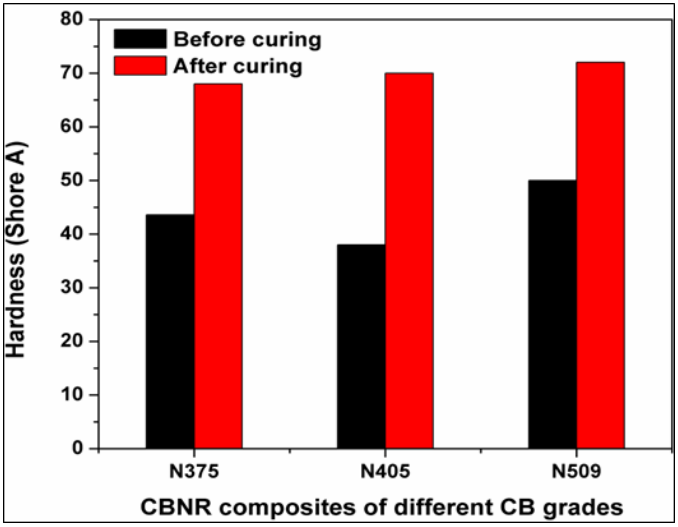

Fig 6: Histogram illustrating Shore Hardness of CBNR composites before and after curing

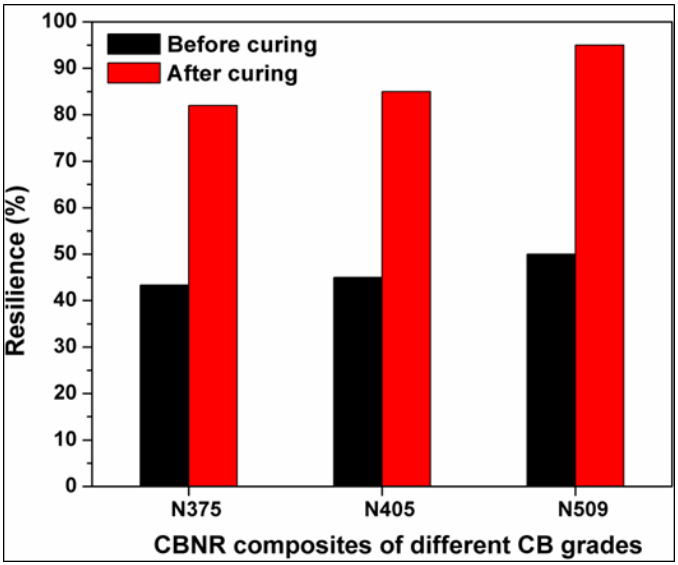

Fig 7: Histogram depicting Resilience of CBNR composites before and after curing

Table 3: Hardness and Resilience for CBNR composites with different grades of CB (N375, N405 and N509) before and after curing

Mechanical Property	N375 CBNR	N405 CBNR	N509 CBNR
Hardness (Shore A) before Curing	43.6	38.0	50.0
Hardness (Shore A) after Curing	68.0	70.0	72.0
Resilience (%) before Curing	43.3	45.0	50.0
Resilience (%) after Curing	82.0	85.0	95.0

5. Swelling studies

Swelling behaviour of the rubber composites was determined by the change in mass by means of method used by Ahmed et. al. The test pieces of known weight (W_b) of vulcanized CBNR composites were immersed in toluene solvent in diffusion test bottles and kept at room temperature for five days. After five days the test rubber samples were removed from the bottles and the wet surfaces were instantly cleaned of liquid via tissue paper swab and re-weighed (W_a). The test rubber samples of the CBNR composites were further evaporated in an oven at 60 °C for 24 hours, cooled in a desiccator and immediately weighed (W_c). Figure. 9 illustrates the flow chart of the method used in this study [17-18].

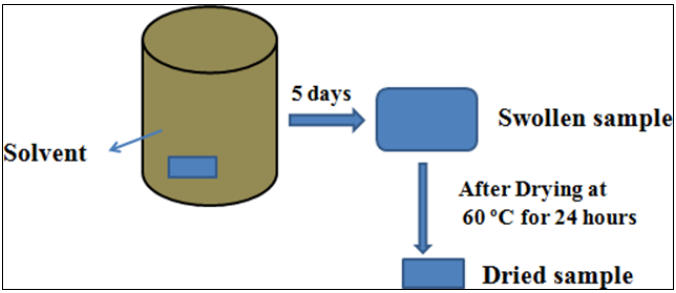

Fig 8: Optical image of swelling studies

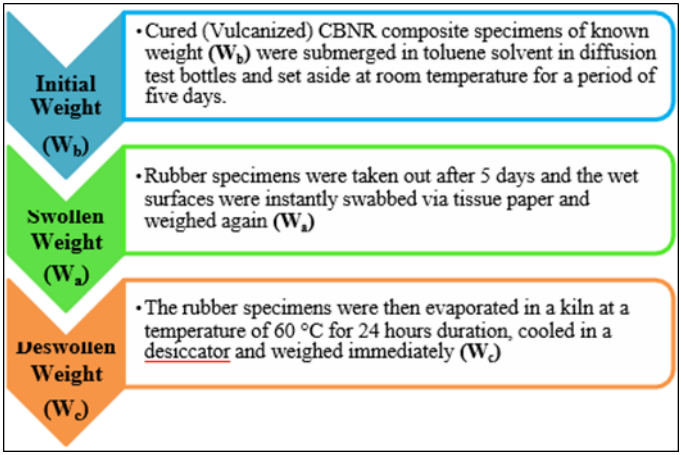

Fig 9: Flow chart depicting the procedure of swelling studies

The swelling parameters of the CBNR composites were computed by the subsequent swelling data and the results are tabulated in Table 4.

i) Swelling index (SI)

Swelling index (SI) was computed by the equation

$$SI\ \% = \frac{Wa - Wb}{W_b} \times 100 \quad (3)$$

ii) Solubility %

Soluble fraction (SF %) was determined by the following relation.

$$SF\ \% = \frac{Wb - Wc}{W_b} \times 100 \quad (4)$$

Where:

W_a = Swollen Weight.

W_b = Initial Weight/dry weight.

W_c = De-swollen Weight.

Table 4: Swelling parameters of CBNR composites

CBNR composite	SI (%)	SF (%)
N375	206.25	4.37
N405	198.34	3.87
N509	195.00	3.50

From the swelling studies, it is seen that N509 showed minimum swelling index and swelling fraction, which indicates maximum cross-linking occurred in N509 CBNR composite among all the three rubber composites (N375, N405 and N509).

6. Morphological and Chemical composition analysis

The three prepared CBNR composites were characterized by SEM in order to see the morphology of the rubber composite. SEM results (Figure 10) showed that CB mainly exists as the aggregates in the rubber matrix. Almost all types of carbon black (N375, N405 and N509) aggregates were observed to be distributed uniformly in the matrix of NR. However, carbon black aggregates size varies with the type of carbon black grade. The filler N509 with large surface area has a small size. It was clearly seen from the SEM micrographs that there is cross-linking occurring in N509 grade CB which justifies its mechanical properties.

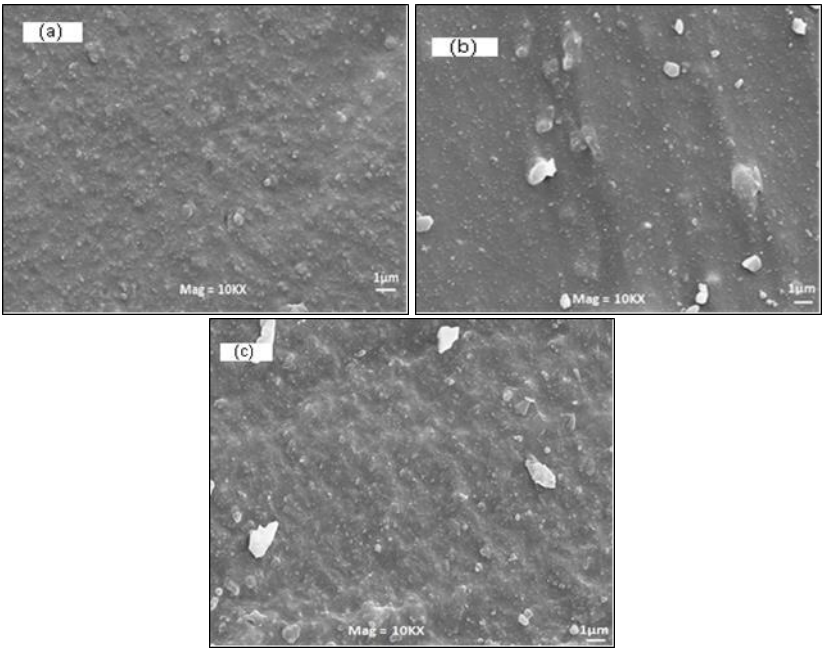

Fig 10i): Secondary electron SEM micrographs of (a) N375 CBNR, (b) N405 CBNR, (c) N509 CBNR composite at 10KX magnification

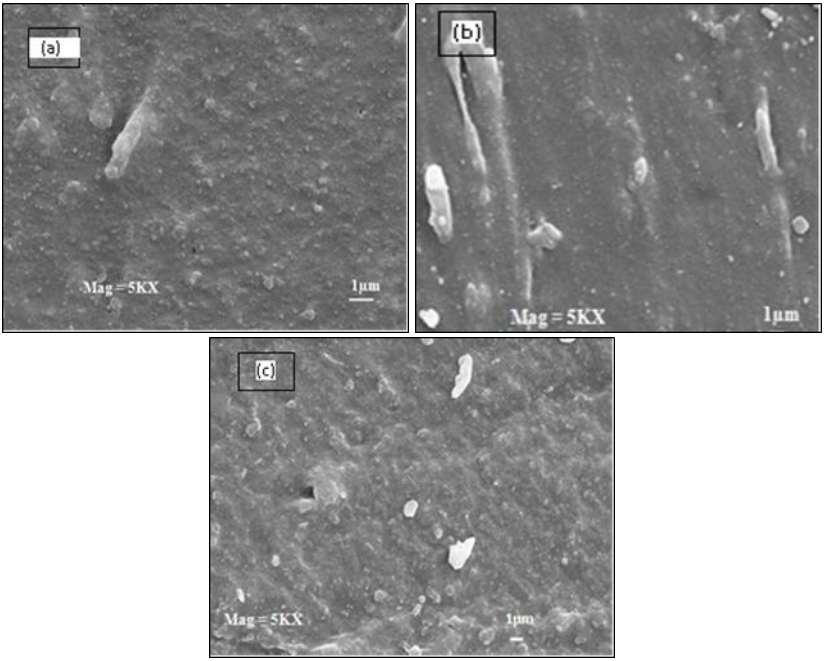

Fig 10ii): Secondary electron SEM micrographs of (a) N375 CBNR, (b) N405 CBNR, (c) N509 CBNR composite at 5KX magnification

7. EDS analysis of CBNR Composites

The three prepared CBNR composites were characterized by EDS to observe the chemical composition of the constituents present in the rubber composites. The EDS spectrums of the composites are illustrated in Figure.11 and the results of chemical composition of the constituents present in the rubber composites are tabulated in Table. 5 and Table.6. It is observed that the content of the cross linking agent Sulfur is found to be maximum in N509 compared to N375 and N405 CBNR composites.

Table 5: Weight % of different elements present in CBNR composites

Element	(N375) Weight %	(N405) Weight %	(N509) Weight %
C	87.37	90.08	91.61
O	7.97	3.94	_
Si	0.22	0.69	1.62
S	1.96	2.34	4.39
Zn	2.49	2.33	2.39
Ca	_	0.61	0.61

Total	100	100	100

Table 6: Atomic % of different elements present in CBNR composites

Element	(N375) Atomic %	(N405) Atomic %	(N509) Atomic %
C	92.32	95.00	96.78
O	6.32	3.12	_
Si	0.10	0.31	0.73
S	0.77	0.93	1.74
Zn	0.48	0.45	0.76
Ca	_	0.19	0.19
Total	100	100	100

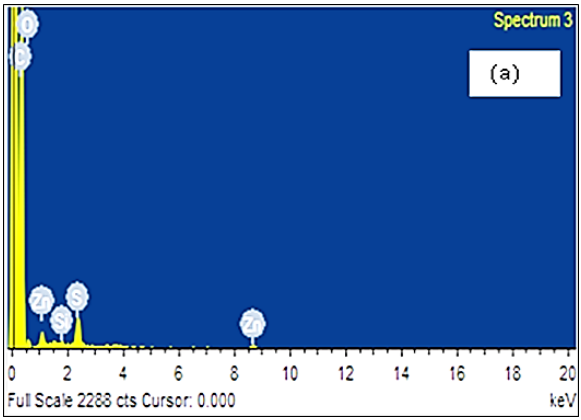

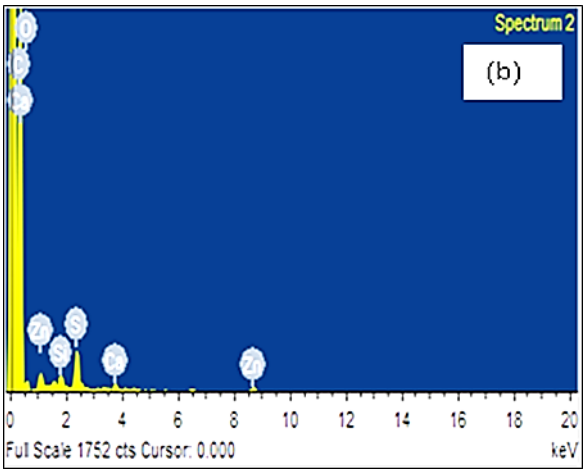

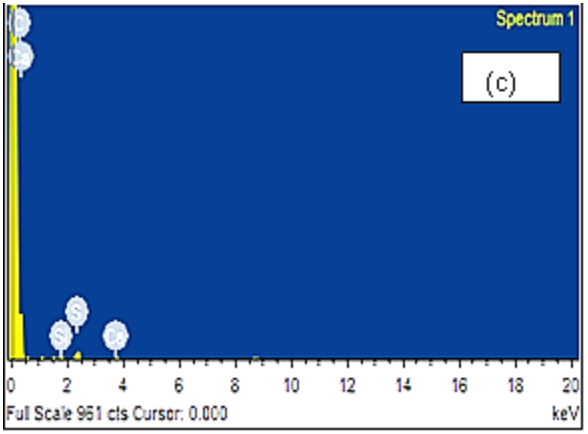

Fig 11: EDS spectrum of (a) N375 CBNR composite (b) N405 CBNR, (c) N509 CBNR composite

Conclusion

The present studies confirmed the significant dependence of mechanical and rheological characteristics of rubber composites on the morphological factors of CB such as surface area, particle size and pellet hardness. These experiments showed a likely direct correlation of tensile strength, resilience and hardness of CBNR composite with the surface area of CB. The decrease in particle size of CB powder additionally reduced modulus of CBNR composite at 200% and 300% elongation. Further, the interconnection of calculated RSF value of CB powders with that of CRI and elongation at break of CBNR composites could be employed to predict the feasibility of different grades of CB for manufacturing CBNR composites. Among the three grades under investigation N509 grade CBNR composite showed highest hardness, resilience, tensile strength which is justified by maximum cross linking of N509 CBNR composite suggested by the SEM and EDS studies.

References

1. Shenderova OA, Gruen DM. Ultrananocrystalline diamond: synthesis, properties and applications: William Andrew, 2012.
2. Kartsova LA, Makarov AA. Properties of Carbon Materials and Their Use in Chromatography, Russian Journal of Applied Chemistry. 2002;75:1725-1731.
3. Donnet JB, Bansal RC, Wang MJ. Carbon black: science and technology. New York: Dekker, 1993.

4. Zhang W, Blackburn R, Dehghani-Sanij A. Effect of carbon black concentration on electrical conductivity of epoxy resin-carbon black-silica nanocomposites, J Mater Sci. 2007;42:7861-7865.

5. Starý Z. Electrical conductivity and rheology of carbon black composites under elongation, AIP Conference Proceedings. 2015;1662:040001.

6. Sahoo BP, Naskar K, Tripathy DK. Electrical Properties of Ethylene Acrylic Elastomer (AEM) Loaded With Conducting Carbon Black, AIP Conference Proceedings. 2011;1349:190-191.

7. El-Tantawy F, Kamada K, Ohnabe H. Electrical properties and stability of epoxy reinforced carbon black composites, Materials Letters. 2002;57:242-251.

8. Azim SS, Satheesh A, Ramu KK, Ramu S, Venkatachari G. Studies on graphite based conductive paint coatings, Prog. Org Coat. 2006;55:1-4.

9. Moteki N, Kondo Y, Nakamura SI. Method to measure refractive indices of small non-spherical particles: Application to black carbon particles, Journal of Aerosol Science. 2010;41:513-521.

10. Rattanasom N, Prasertsri S. Relationship among mechanical properties, heat ageing resistance, cut growth behaviour and morphology in natural rubber: Partial replacement of clay with various types of carbon black at similar hardness level, Polymer Testing. 2009;28:270-276.

11. Coran AY. Chemistry of the vulcanization and protection of elastomers: A review of the achievements, Journal of Applied Polymer Science. 2003;87:24-30.

12. Ponnamma D, Maria H, Chandra A, Thomas S. Rubber Nanocomposites: Latest Trends and Concepts, in Advances in Elastomers II. Visakh PM, Thomas S, Chandra AK, Mathew AP, Eds., ed.: Springer Berlin Heidelberg. 2013;12:69-107.

13. Donnet JB. Nano and microcomposites of polymers elastomers and their reinforcement, Composites Science and Technology. 2003;63:1085-1088.

14. Vilgis TA. Time scales in the reinforcement of elastomers, Polymer. 2005;46:4223-4229.

15. Kohls DJ, Beaucage G. Rational design of reinforced rubber, Current Opinion in Solid State and Materials Science. 2002;6:183-194.

16. Heinrich G, Klüppel M, Vilgis TA. Reinforcement of elastomers, Current Opinion in Solid State and Materials Science. 2002;6:195-203.
17. Bhattacharya M, Bhowmick A. Synergy in carbon black-filled natural rubber nanocomposites. Part I: Mechanical, dynamic mechanical properties and morphology, J Mater Sci. 2010;45:6126-6138.
18. Edwards DC. Polymer-filler interactions in rubber reinforcement, J Mater Sci. 1990;25:4175-4185.
19. Litvinov VM, Steeman PAM. EPDM-Carbon Black Interactions and the Reinforcement Mechanisms, As Studied by Low-Resolution 1H NMR, Macromolecules. 1999;32:8476-8490.